

Faculty of Physics and Astronomy

University of Heidelberg



Diploma thesis

in Physics

submitted by

Bastian Martin Märkisch

born in Ruit auf den Fildern

2002

**Studies on CASCADE Detector Prototypes
and
Development of its Infrastructure**

This diploma thesis has been carried out by Bastian Martin Märkisch at the
Physics Institute, Heidelberg
under the supervision of
Priv.-Doz. Dr. Hartmut Abele

Abstract

The CASCADE detector provides a new concept for the detection of thermal and cold neutrons. Cascaded GEM-foils coated with the solid neutron converter ^{10}B increase the detection efficiency while preserving the spatial resolution of the neutron conversion.

In this diploma thesis several prototypes of the CASCADE detector were designed, manufactured and tested successfully. Amongst them is a beam monitor for the Small Angle Neutron Scattering facility (SANS) at the Paul-Scherrer-Institut (PSI), Switzerland. In future this detector will be used to monitor the neutrons in the direct beam and will thus provide a normalisation to the scattering experiments.

The electronics to control the detector and the electronics to process the detector signals were replaced and standardised completely in the course of the work. A system based on the VMEbus yields full control over the essential operational parameters of the detector. A software library was especially designed for that purpose.

Time of flight measurements at beam site PF1 at the Institute Laue-Langevin (ILL), France, demonstrated the high rate capability of CASCADE detectors. These measurements allow for an estimation of the neutron flux at $\lambda = 8.9 \text{ \AA}$.

Zusammenfassung

Der CASCADE Detektor ist ein neuartiger Detektor zum Nachweis thermischer und kalter Neutronen. Er basiert auf GEM Folien, die mit dem festen Neutronenkonverter ^{10}B beschichtet sind. Durch Kaskadierung dieser Folien wird die Nachweisefizienz für Neutronen erhöht, wobei die Ortsinformation der Detektion vollständig erhalten bleibt.

Im Rahmen dieser Arbeit wurden mehrere Prototypen des CASCADE Detektors entworfen, gebaut und erfolgreich getestet, unter ihnen ein Strahlmonitor für die Kleinwinkelstreuanlage (SANS) am Paul-Scherrer-Institut (PSI), Schweiz. Dieser soll in Zukunft die Messungen dieser Anlage vervollständigen.

Die Steuer- und Ausleelektronik des Detektors wurde während dieser Arbeit weitgehend erneuert und in diesem Zuge vereinheitlicht. Ein System basierend auf dem VMEbus ermöglicht mit Hilfe einer eigens entwickelten Software-Bibliothek die vollständige Kontrolle über die wesentlichen Betriebsparameter des Detektors.

Bei Flugzeitmessungen am Strahlplatz PF1 am Institute Laue-Langevin (ILL), Frankreich, wurde erstmalig die hohe Ratentauglichkeit der CASCADE Detektoren unter Beweis gestellt. Aus diesen Messungen ergibt sich eine Abschätzung des Neutronenflusses an diesem Strahlplatz bei $\lambda = 8.9 \text{ \AA}$.

Contents

1	Introduction	1
2	Concept of the CASCADE Detector	3
2.1	Neutron Converters	3
2.2	^3He Counter Tube	4
2.3	Solid Neutron Converters in Gas Detectors	6
2.4	Gas Electron Multiplier (GEM)	8
2.5	The CASCADE Detector	9
2.5.1	Detection Efficiency	10
2.5.2	Spatial Resolution	12
2.5.3	Counting Gas	12
2.5.4	Readout Structure	12
3	Detector Construction and Infrastructure	15
3.1	Detector Construction and Design	15
3.1.1	Material Selection for Neutron Detectors	17
3.1.2	Material Testing	20
3.2	Electronics and Software	25
3.2.1	The New Hardware Concept	25
3.2.2	The CIPix Chip	27
3.2.3	FPGA Board	29
3.2.4	Hardware Access Library	29
4	Detector Prototypes and Measurements	33
4.1	Detector Prototypes	33
4.1.1	The Beam Monitor for SANS at the PSI	33
4.1.2	PSI Prototype	39
4.1.3	ILL Prototypes A and B	40
4.2	Characterisation of the Prototypes	42
4.2.1	Efficiency Measurements	42
4.2.2	Spatial Resolution	45
4.2.3	Effective Dead Time Estimation	46
4.2.4	Rate Capability Tests	48
4.3	Time of Flight Measurements at PF1	49
4.3.1	Time of Flight Measurements (TOF)	49

4.3.2	Experimental Setup at PF1	49
4.3.3	Neutron Flux	49
4.3.4	Experimental Results	56
5	Summary and Outlook	59
A	Bus system glossary	61
A.1	VMEbus	61
A.2	CAN bus	61
A.3	I ² C-bus	62
B	Drawings of the SANS beam monitor housing	63

1 Introduction

The neutron was discovered by Chadwick in 1932. Since then the neutron has not only been of interest to fundamental physics but is also used as a tool to provide an insight into the solid state of matter as well as its dynamics. It has proved invaluable for today's scientific view of the world.

Currently several new intense neutron sources are either planned or already under construction around the globe: the European Spallation Source in Europe (ESS), the Spallation Neutron Source in the United States of America (SNS) and the Japanese Spallation Neutron Source (JSNS) in Japan. Compared to what is available today with the most intense neutron source at the Institute Laue-Langevin (ILL) in France, these pulsed sources will offer peak intensities that are about three orders of magnitude higher. Scientific neutron scattering instruments at these pulsed sources will need detectors with an excellent time resolution to take advantage of the given time structure in the beam. Moreover, detectors will need to cope with instantaneous intensities which are much higher than known today. All of these modern neutron sources are projecting instruments with large-area neutron detectors on the order of 10 m^2 each. Current neutron detector technology either fails to fulfil the majority of these characteristics, or is it impossible to manufacture detectors with sizes of this scale.

The CASCADE project aims to resolve these issues. The CASCADE detector combines reliable and established technology of Gas Electron Multiplier (GEM) foils with a solid neutron converter. GEM-foils are employed as a substrate for the neutron converter material boron-10 (^{10}B). Consequently a GEM-foil is opaque for neutrons while transparent for charges. This property allows to overcome the usual limitations with solid converter materials: an insufficient detection efficiency of a single converter coating. Being transparent for charges, several such coated GEM-foils can be cascaded successively. Thence an increase in detection efficiency is achieved while charges can be channelled through the layers and accumulated on a readout structure behind the stack. As the counting gas is not used as neutron converter but solely serves to transfer the charges, the detector can be operated at ambient pressure. Furthermore, the rate capability of the CASCADE detector is inherently high due to the micro-structures involved. In comparison, standard ^3He gas-detectors need high gas pressure to obtain an appreciable detection efficiency. Thus, their rate capability is limited and heavy, bulky pressure tanks are needed. These detectors are not scalable to large area, high count rate detectors.

The concept of the CASCADE detector is introduced in chapter 2. The underlying physical mechanisms are explained. The comparison to conventional neutron

detectors shows the advantages of this new detector concept. Chapter 3 describes the mechanical design of the detector and the detector infrastructure, including hard- and software. It includes investigative neutron transmission and scattering measurements on GEM-foils. Additionally the transfer of signal readout technology from high energy physics into the neutron sector is illustrated. In chapter 4 prototypes of the CASCADE detector are described in detail. These include the new beam monitor for the Small Angle Neutron Scattering (SANS) site at the Paul-Scherrer-Institut (PSI). As part of this work detectors were designed and built in Heidelberg and characterised at the PSI and the Institute Laue-Langevin (ILL). Furthermore, the experimental results of time-of-flight measurements at the PF1A site at the ILL are presented. Finally, chapter 5 summarises the results obtained in this diploma thesis and describes the plans for the future development of the project.

2 Concept of the CASCADE Detector

The CASCADE detector is designed for detection of thermal and cold neutrons. It is a gas detector based on layers of solid ^{10}B as neutron converter. GEM foils are used as a charge and neutron transparent substrate for these layers. Several GEM foils are combined to form a cascade. The design of the detector results in some remarkable features:

- a rate acceptance exceeding 1 MHz cm^{-2}
- large sensitive area of up to $30 \times 30 \text{ cm}^2$ per detector module with little blind area
- manufacturable on large scales and robust technology
- neutron detection efficiency of up to 50 % for thermal neutrons
- time resolution better than $1 \mu\text{s}$

These characteristics make it a promising candidate for application at the new spallation neutron sources. These sources feature high neutron fluxes and their pulsed beams increase the demand on the time resolution.

This chapter describes the concept of the CASCADE detector. It is compared to the ^3He counter tube, which is a technology still widely in use today.

2.1 Neutron Converters

Neutrons do not carry an electric charge and can therefore not be detected directly through ionisation processes. Instead, so called neutron converter materials are used. The nuclei of these materials capture neutrons and in consequence emit charged particles as products of a prompt nuclear reaction. These particles can then be detected by using well known techniques such as gas detectors or scintillation detectors.

Isotopes which have a large cross section for neutron absorption are listed in table 2.1. This table also includes the corresponding nuclear reactions and the energy of the conversion particles. For thermal and cold neutrons this energy is independent from the energy of the incident neutron, whereas the absorption cross section σ_a scales linearly with the wave length λ of the neutrons.

Two categories of converters may be distinguished: gas converters like ^3He and $^{10}\text{BF}_3$ and solid converters like ^{10}B , ^6Li and the gadolinium isotopes.

${}^3\text{He} + n \longrightarrow {}^3\text{H} + p + 764 \text{ keV}$	$\sigma_a = 5330 \text{ barn}$
${}^6\text{Li} + n \longrightarrow {}^3\text{H} + \alpha + 4.78 \text{ MeV}$	$\sigma_a = 940 \text{ barn}$
${}^{10}\text{B} + n \xrightarrow{6\%} {}^7\text{Li} + \alpha + 2.79 \text{ MeV}$	$\sigma_a = 3835 \text{ barn}$
$\xrightarrow{94\%} {}^7\text{Li}^* + \alpha + 2.31 \text{ MeV}$	
$\longrightarrow {}^7\text{Li} + \gamma (0.48 \text{ MeV})$	
${}^{155}\text{Gd} + n \longrightarrow {}^{156}\text{Gd}^*$	$\sigma_a = 61000 \text{ barn}$
$\longrightarrow {}^{156}\text{Gd} + \gamma + e^- (29 - 181 \text{ keV})$	
${}^{157}\text{Gd} + n \longrightarrow {}^{158}\text{Gd}^*$	$\sigma_a = 254000 \text{ barn}$
$\longrightarrow {}^{158}\text{Gd} + \gamma + e^- (29 - 181 \text{ keV})$	
${}^{235}\text{U} + n \longrightarrow \text{fission products} + \approx 160 \text{ MeV}$	$\sigma_a = 680 \text{ barn}$
${}^{239}\text{Pu} + n \longrightarrow \text{fission products} + \approx 160 \text{ MeV}$	$\sigma_a = 1017 \text{ barn}$

Table 2.1: Neutron converters and the respective nuclear reaction. σ_a is the cross section for absorption of thermal neutrons ($\lambda_0 = 1.8 \text{ \AA}$)

2.2 ${}^3\text{He}$ Counter Tube

${}^3\text{He}$ is the converter most commonly used today. The most simple detector which employs this converter is the ${}^3\text{He}$ proportional counter tube. It is described here exemplarily as a representative for this category of neutron detectors, which includes multi-wire proportional counters (MWPC) and microstrip detectors (MSGC). Details on these technologies are given in [Kle00].

The ${}^3\text{He}$ counter tube consists of a metal tube filled with gaseous ${}^3\text{He}$. A thin wire in the middle of the tube is used as an anode for a high voltage (which is of the order of 1 kV). The geometry of the counter tube can be seen in figure 2.1.

The ${}^3\text{He}$ gas is used as converter and counting gas at the same time. Neutrons

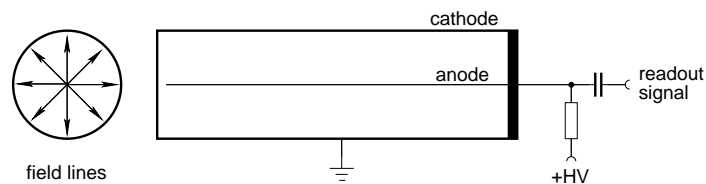


Figure 2.1: Schematic of the ${}^3\text{He}$ proportional counter tube. The typical diameter of the tube is between 2 and 5 cm

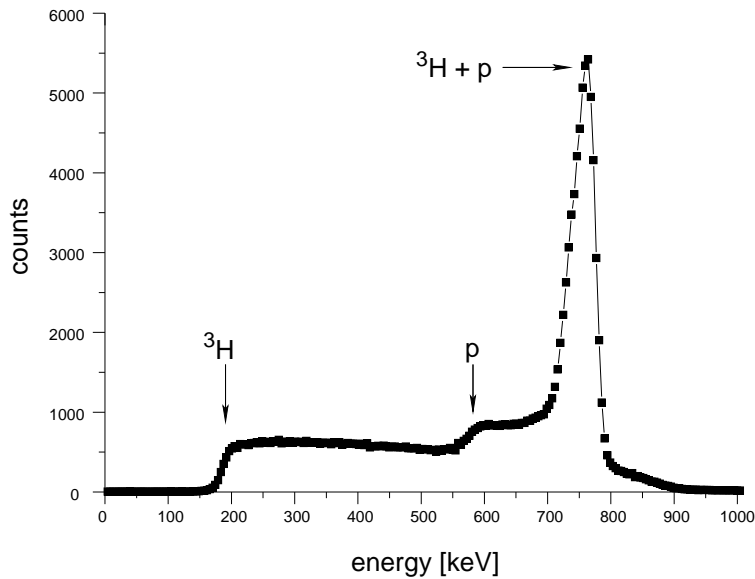


Figure 2.2: Typical pulse height spectrum of a ^3He counter tube. At the minimum energy of 191 keV the ^3H ions deposit their energy completely in the counting gas. This is used to set up a stable energy discrimination.

captured by a ^3He nucleus cause a nuclear reaction as shown in table 2.1. The products then ionise atoms of the surrounding counting gas. The resulting electron/ion pairs are accelerated towards the anode and the cathode, respectively, by the gradient of the electric field. Close to the anode the electrons are accelerated sufficiently to cause gas amplification by ionisation of further gas atoms.

The resulting pulse is coupled out from the anode by a capacitor. A typical pulse height spectrum can be seen in figure 2.2. The shape of the spectrum is caused by so called ‘boundary effects’, when protons and tritium nuclei only deposit a fraction of their total energy in the counting gas before hitting the walls of the counting tube. The spectrum has a finite minimum energy. This is the kinetic energy of the ^3H nucleus. This limit is used to discriminate safely between detection signals and background noise.

To obtain high neutron detection efficiencies of $\approx 100\%$, the detector has to be filled with ^3He at a pressure of up to 10 bar. The drift velocity v_d of the ions in the counting gas is anti-proportional to the pressure p of the gas. Therefore, a higher gas pressure extends the signal duration time. A higher detection efficiency has thus to be traded against count rate acceptance. Typical ^3He counter tubes have a rate acceptance of the order of 10 kHz. Additionally, the high gas pressure makes detectors covering large areas impractical, since they would require a massive detector housing. Thick entrance windows of the detectors absorb and scatter neutrons and

thereby influence measurements.

The spatial resolution of the ^3He counter tube is clearly limited by the size of the tube. At present prototypes are developed at the ILL which have a better spatial resolution as a consequence of the reduction of the diameter of the tube. The resolution along the wire is increased by application of charge division techniques. These detectors obtain a spatial resolution of ~ 7 mm.

Another important feature of any detector is its time resolution. In neutron physics good time resolution is required for investigations on the dynamical properties of condensed matter (e. g. phonons) and is a necessity for the efficient usage at spallation sources with their pulsed beams. For these purposes the energy of the neutron has to be determined. This is commonly done by time-of-flight (TOF) measurements. For accurate TOF measurements, both, the flight time and the exact flight path have to be known. Modern electronics are capable of highly accurate time measurements, whereas the determination of the flight path is limited to the uncertainty of the location of the neutron conversion. This uncertainty is due to the depth of the neutron converter. Conversion processes can take place anywhere within the converter material. Therefore, the time resolution of ^3He counter tubes is limited to ~ 10 μs . This corresponds to the time it takes thermal neutrons ($v \approx 2000$ m s^{-1}) to pass through a typical counter tube with $\phi = 2$ cm.

2.3 Solid Neutron Converters in Gas Detectors

Neutron detectors which are based on ^3He as neutron converter have restrictions on rate acceptance and spatial resolution as described in the last section. These restrictions can be lifted by using solid neutron converters such as ^{10}B or ^6Li .

Solid neutron converters have various advantages. They separate the neutron conversion process from the detection of the conversion products. In contrast to counter tubes filled with ^3He this allows the use of cheap counting gases like, e. g. a mixture of argon and carbon dioxide instead of the precious ^3He gas. Hence, a continuous flow of counting gas through the detector is made affordable. This constant exchange of gas removes all contaminants from the counting gas. Ageing effects like a decrease in the detection efficiency due to chemical reactions are reduced considerably.

In contrast to detectors using gas converters the detection efficiency of neutron detectors which are based on solid converters no longer depends on the pressure of the counting gas. It is only dependent on the thickness of the converter layers. For the CASCADE detector ambient gas pressure is sufficient. It eliminates the need for massive detector housings and makes detectors possible which are cover a large area.

Another advantage of solid converters is their high density, which is about four orders of magnitude higher than that of gas converters. The location of the neutron conversion is only limited by the thickness of the converter layer. This makes excellent time resolutions possible. A thickness of the converter layer of ~ 1 μm results in

a theoretical time resolution of 0.5 ns. The time resolution of the complete detector system is dominated by other processes, such as drift times of the electrons in the counting gas.

The finite range of the conversion particles within the converter is one of the reasons why solid neutron converters are not commonly used. An increase of the thickness of the conversion layer leads to an increased conversion probability, whereas the probability that the conversion products leave the layer is decreased. This limits the efficiency of a single converter layer.

The maximum efficiency of a single layer of e. g. ^{10}B is $\sim 5\%$ for thermal neutrons ($\lambda = 1.8 \text{ \AA}$). This value is very low compared to the efficiency of ^3He counter tubes (up to $\sim 100\%$). The **CASCADE** detector solves this limitation by cascading several layers of boron with the help of **GEM**-foils. This concept is explained in section 2.5.

The conversion particles lose energy by interaction with the converter atoms. The discrete energy spectrum of the conversion particles is turned into a continuous spectrum. In contrast to the energy spectrum of ^3He , it does not have a minimum energy.

According to table 2.1 there are three practical solid neutron converters:

- ^6Li : Lithium is chemically very reactive and therefore very difficult to handle. Its sensitivity to gamma radiation is low due to its low atomic number $Z = 3$, as explained below. The cross section for absorption of neutrons is low when compared to ^{10}B and Gd . However, the energy of the conversion products is high, which results in a large range within the conversion layer. Hence, a single layer of ^6Li has an efficiency slightly larger than a layer of ^{10}B . A major drawback of the large energy of the conversion particles and therefore a large range in the counting gas is the low spatial resolution of the detector.
- Gd : Gadolinium has an extremely high cross section for neutron capture, which results in the highest conversion efficiency of a single layer. Yet its large atomic number $Z = 64$ makes the emission of electrons due to photo effect highly probable. Its conversion products are electrons of rather low energy, which may be difficult to distinguish from photo electrons (see table 2.1). Detectors based on gadolinium are therefore expected to be sensitive to gamma radiation.¹
- ^{10}B : Boron is chemically inert. The mechanical and chemical properties of these boron layers do not change in time because boron does not interact with the substrate or with any counting gas. This leads to stable conditions for detectors based on boron. The cross section of ^{10}B $\sigma_a = 3835$ barn for neutron absorption is moderately large. Its sensitivity to gamma radiation is low due to its low atomic number $Z = 5$. The lower energy of the conversion particles leads to a much better spatial resolution if compared to ^6Li .

¹There is an ongoing research project at the Hahn-Meitner-Institut, Berlin, on neutron detectors which use gadolinium as converter material. [\[HMI\]](#)

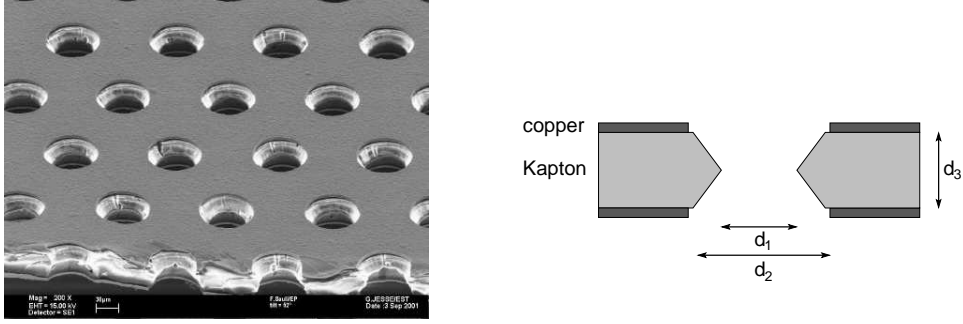


Figure 2.3: Microscopic photograph of a GEM-foil [Sau01]. The geometry of the holes used for the CASCADE detector is currently the same as that used by HERA-B: $d_1 = 55 \mu\text{m}$, $d_2 = 95 \mu\text{m}$ and $d_3 = 50 \mu\text{m}$, the copper layers are $\approx 7 \mu\text{m}$ thick. The distance between two holes is $l = 140 \mu\text{m}$.

As a consequence of the positive and negative properties of the converters mentioned, the CASCADE detector will use layers of ^{10}B as neutron converter.

2.4 Gas Electron Multiplier (GEM)

The GEM-foil was developed by F. Sauli in 1997 at CERN [Sau97]. It is a thin polyimide foil coated with copper on both sides which has been chemically pierced with a periodical grid of holes. The result can be seen in figure 2.3.

The upper and lower side of the GEM have no electrical contact. Application of high voltage yields an electrical field as represented in figure 2.4. Within the holes of the GEMs sufficiently high electrical fields can be generated to cause gas amplification. Gain factors of up to 10^4 can be obtained [Ber98].

In the CASCADE detector these high amplification factors are not needed. Most of the GEMs used are operated in transparent mode, i. e. with a gain factor of about one. In this mode charges are transferred from one side of the GEM to the other without the loss of the information regarding the lateral positioning.

Only the GEMs adjacent to the readout structure are driven in amplification mode with a moderate gain of the order of 10. In this regime sparking does not occur.

The GEM is a robust technology which is employed successfully for a variety of experiments. HERA-B, for example, uses them in combination with microstrip readout structures to obtain high gain factors. In studies to LHCb [Zie99] and in the COMPASS experiment [Sim01] it was proven that GEM-foils can also be successfully used in a cascaded setup.

The GEM-foil has proven to be insensitive to ageing effects and is capable of high event rates of up to 10^7 Hz cm^{-2} [Bre99]. Moreover GEM foils are nearly transparent for neutrons, as shown in section 3.1.2.

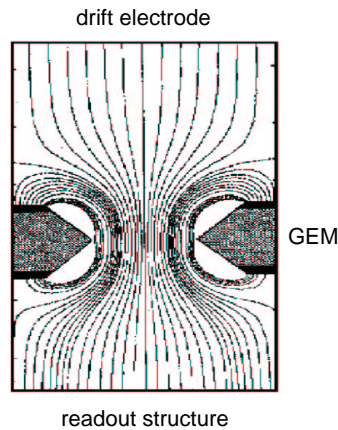


Figure 2.4: Electric field produced by a GEM [Cwe00].

2.5 The CASCADE Detector

The CASCADE detector is designed to be an efficient and position sensitive detector for thermal and cold neutrons on large areas. The detector concept is based on solid neutron converter layers in a common gas detector system. High detection efficiency is reached by cascading several solid neutron converter layers each coated onto a GEM foil, which is used as charge and neutron transparent substrate. This setup is depicted in figure 2.5.

Incident neutrons can be absorbed by one of the boron layers in the detector. One of the conversion products of the neutron capture, a ${}^7\text{Li}$ nucleus or an alpha particle, leaves the conversion layer and enters the gas volume. There it deposits its kinetic energy producing electron/ion pairs. The electrons are transferred through the stack towards the readout structure by a drift field. This is made possible by the transfer-GEMs, which are operated in transparent mode. The positional information of the event is not distorted and there is no overall gas amplification.

The last GEM adjacent to the readout structure, the so called gain-GEM, amplifies the signal by a factor of ~ 10 . An average of about 10^5 electrons will reach the readout structure per conversion event. A passive readout structure is sufficient to extract these charges.

A remarkable feature of this concept is the complete separation of all stages of the neutron detection. The absorption and conversion of the neutrons does no longer influence the gas detection of the fragmentation products (independent from the pressure and mixture of the counting gas). Additionally, the gas amplification by the gain-GEM is independent from the design of the readout structure. It can be optimised for the needs of a specific application. Possible designs include stripes, pixel patterns or circular ring patterns for the integration over Laue-diffraction-rings.

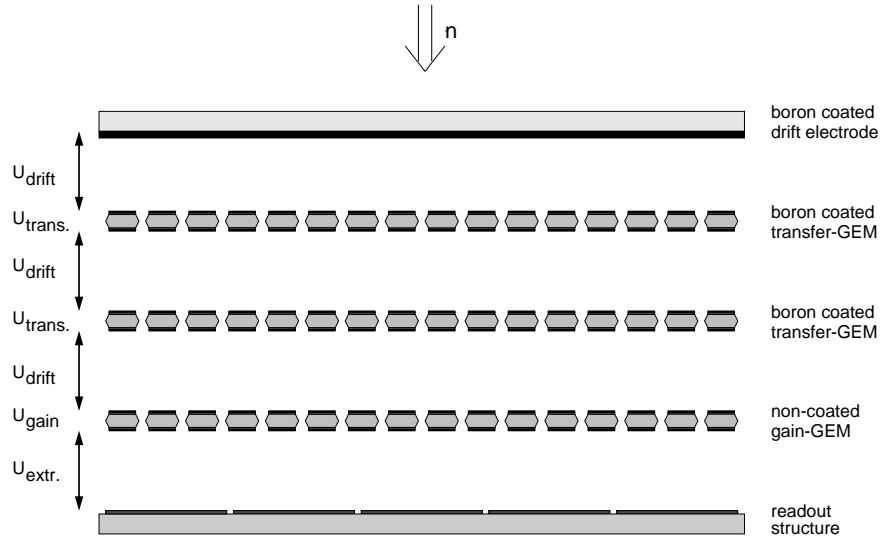


Figure 2.5: Sketch of a CASCADE detector with 3 GEM-foils and 5 layers of ^{10}B .

The next sections will discuss some further details of the design of the CASCADE detector. Measurements on the counting gases are presented in [Bru02]. The spatial resolution is discussed in detail in [Kle00]. Only brief explanation will be given here.

2.5.1 Detection Efficiency

Figure 2.6 shows the efficiency of a single layer of ^{10}B on a substrate for thermal neutrons. In the *forward case* the neutrons penetrate the substrate before entering the conversion layer. As the conversion products cannot penetrate the substrate, they only leave the conversion layer in the direction of the neutron beam. In the case where the neutrons enter the conversion layer first, the *backward case*, this situation is reversed and the conversion particles are emitted in the opposite direction to the incident neutron beam. Detailed calculations on the neutron detection efficiency in [Kle00] and [Bru02] show that the detection efficiency of a single layer of ^{10}B is limited to $\sim 5\%$ for thermal neutrons. This is due to the finite range of the conversion particles in boron.

In the CASCADE detector both of the above cases are used together. The boron layer on the drift electrode, for example, is an example of the *forward case*. The combination of all boron layers results in an increased total neutron detection efficiency. For 20 layers of ^{10}B an efficiency of 50% is obtained. This corresponds to 10 GEM-foils coated on both sides. For most applications in neutron physics an efficiency of 50% will suffice. Figure 2.7 depicts the detection efficiency obtainable by different numbers of boron layers.

A plot of the wave length dependency of the neutron detection efficiency is shown

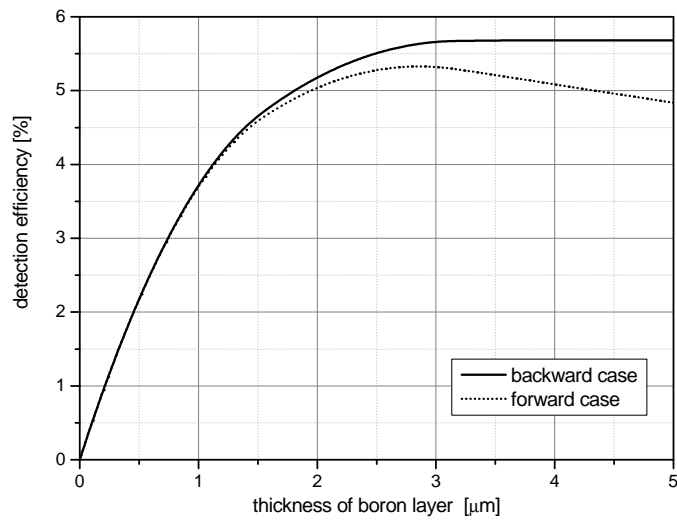


Figure 2.6: Detection efficiency for thermal neutrons using a single layer of ^{10}B on a substrate. Two cases are distinguished: in the *forward case* and the *backward case*, depending on if the neutrons penetrate the substrate first or not. [Kle00], [Bru02]

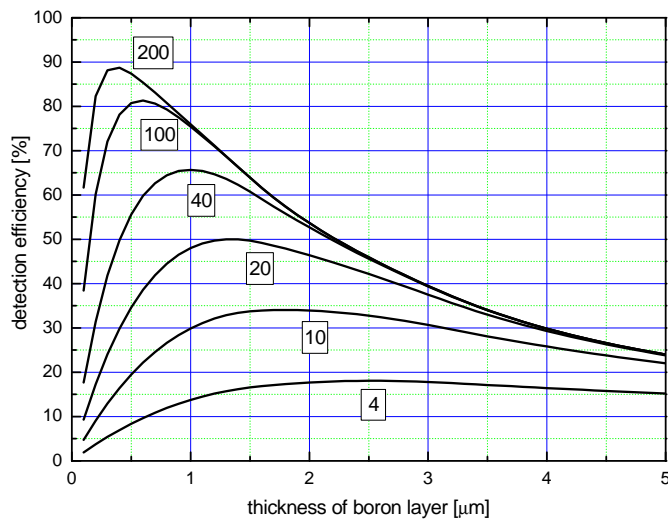


Figure 2.7: Detection efficiency for thermal neutrons of the CASCADE detector as a function of the thickness of the boron layers. Different curves represent a different number of boron layers. All layers have the same thickness.

in figure 4.9. It describes one of the prototypes built as part of this thesis.

2.5.2 Spatial Resolution

The spatial resolution of the CASCADE detector is determined by the range of the conversion products in the counting gas. This range is 2 to 6 mm, depending on the stopping power of the counting gas used. The transversal expansion of the electron cloud is negligible compared to the range of the conversion particles.

Preliminary tests, as described in section 4.2.2, showed that the resolution measured is consistent with simulations carried out in [Kle00].

2.5.3 Counting Gas

The decoupling of the neutron conversion process from the detection of the converter particles allows cheap counting gases to be used in the CASCADE detector. Current prototypes use the well known combination of argon and carbon dioxide or tetra fluor methane.

Experiments discussed in [Bru02] showed that a mixture of argon and carbon dioxide of 90 : 10 yield a stable and efficient conditions. No ageing of the detector is caused by this gas mixture, even so at high counting rates [Kol01].

CO₂ is preferred over CF₄ for the prototypes, since its considerably cheaper. All measurements in chapter 3 and 4 use this gas combination.

2.5.4 Readout Structure

The strong ionisation signals of the conversion products of ¹⁰B and the amplification by the gain-GEM eliminate the need for an amplifying readout structure, such as the microstrip technology. Instead a passive readout structure can be used, which is much more robust and insensitive to ageing processes.

A simple printed circuit board (PCB) is used as readout structure for the CASCADE detector. At the moment only one dimensional structures are available. These consist of stripes of gold on a polyimid foil as substrate. The stripes have a width of 2.8 mm and are separated from each other by 0.2 mm. Two dimensional readout structures are currently developed. These will have two separate sets of stripes, one for every readout dimension.

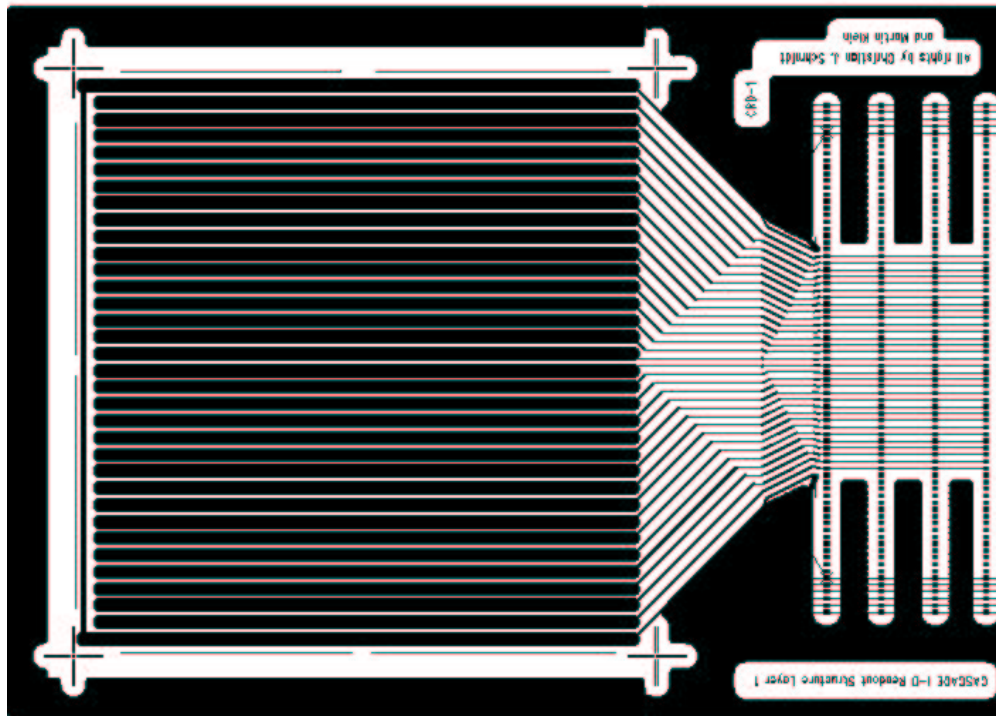


Figure 2.8: Sketch of the one dimensional readout structure of the CASCADE detector as used for the PSI and ILL prototypes. The readout stripes in the middle are constricted to the width of a standardised connector. In the future they will be directly connected to the readout board AS10 [EW] which is shown in figure 3.9 [Sch02].

3 Detector Construction and Infrastructure

The construction of a CASCADE detector requires a careful selection of materials and mechanical setup to minimise neutron scattering within the detector itself as well as to maximise its detection efficiency. Section 3.1 describes the current design of the detector. It also includes details on material tests that have been carried out at the Paul-Scherrer-Institute, Switzerland (PSI).

Furthermore, the large amount of readout channels, high counting rates and the continuous gas flow demand a more sophisticated infrastructure than needed for ^3He counter tubes for example. Section 3.2 explains the concept of the detector infrastructure, including soft- and hardware. Figure 3.1 gives an overview of the functional modules.

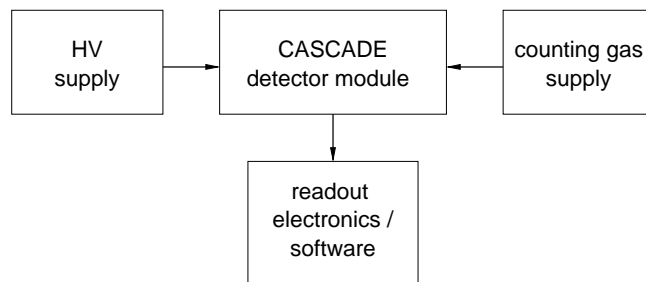


Figure 3.1: Overview of the infrastructure of the CASCADE detector

3.1 Detector Construction and Design

The current design of the CASCADE detector addresses several aspects:

- All parts of the detector that will be exposed to neutrons, with exception of the boron conversion layers, should not scatter or absorb neutrons. More criteria for material selection are given in section 3.1.1. Several materials considered for usage in the detector were tested. The results of these tests are discussed in section 3.1.2.

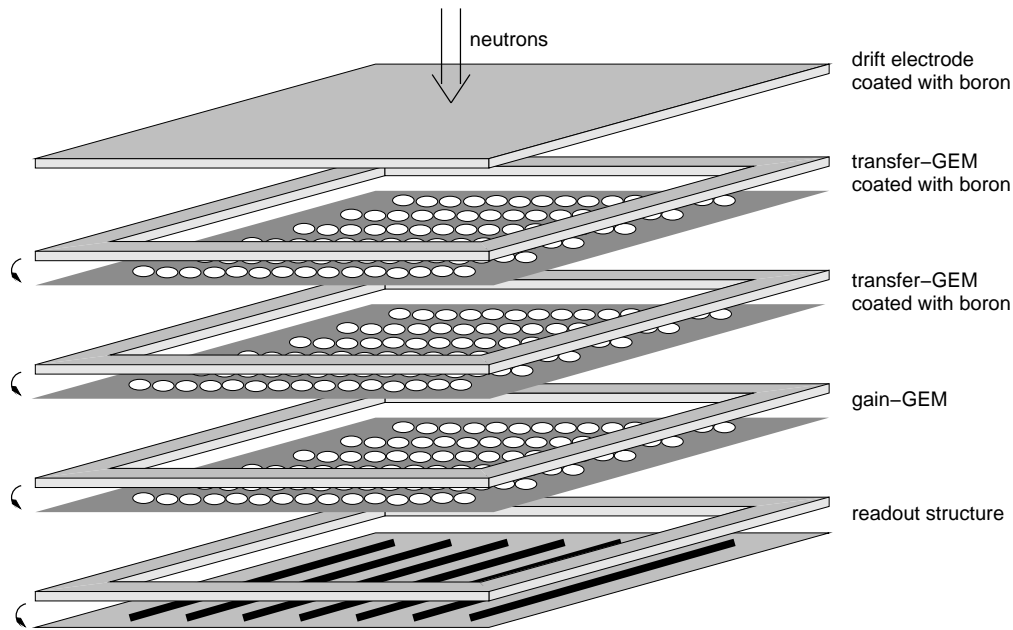


Figure 3.2: Modular design of the CASCADE detector. The GEMs (and the readout structure) are glued to frames.

- Ageing effects, which have direct impact upon detector stability and life-time, strongly depend on hydrocarbon or silicon contaminants [Cap01]. Thus minimising ageing effects implies the avoidance of any outgassing materials in the detector.
- The mechanical setup of the detector should take manufacturing aspects as well as service aspects into account.

The construction of the CASCADE detector is based on a modular concept. The basic units of the detector are GEM-foils which have been stretched and glued onto frames. This concept is demonstrated in figure 3.2. The foils labelled *transfer-GEM* are coated with boron on both sides, whereas the foil labelled *gain-GEM* is coated on the opposite side of the readout structure only, or not even coated at all. The readout structure currently consists of a simple, flexible, printed circuit board which is also glued onto a frame.

The resulting modules are stacked one upon another to form a detector stack. This stack is held in place and pressed together by screws. Between every two frames a thin teflon foil of the same shape as the frame is placed to prevent gas leakage. The resulting detector is not necessarily gastight. It does not have to be, since the detector is operated with gas flowing through it continuously. This removes any undesired contaminants from the detector and thereby prevents ageing of the detector. Continuous purge of counting gas is a feasible alternative as the

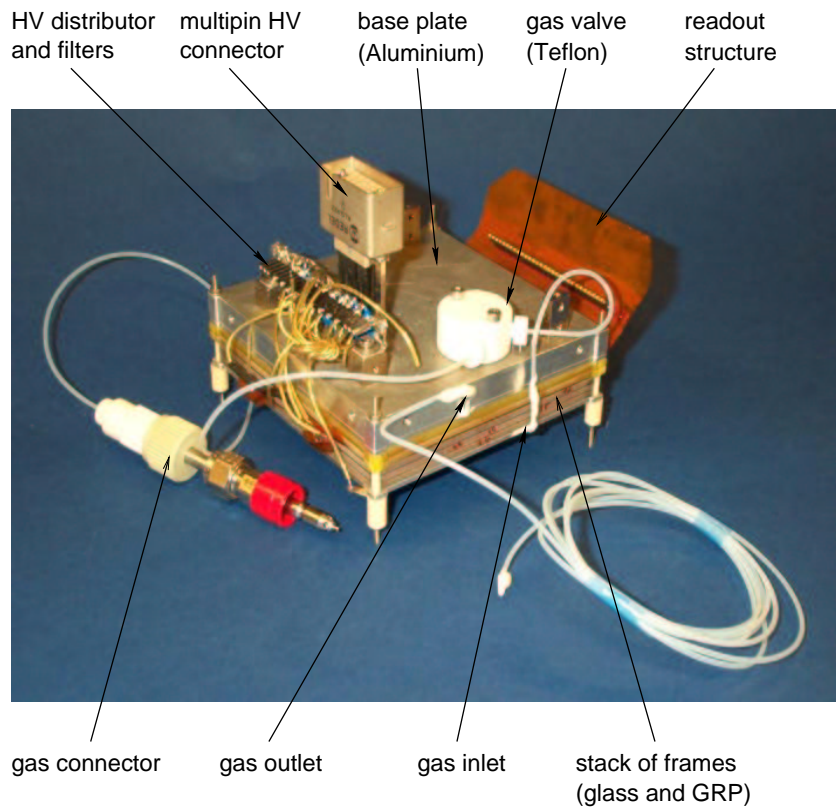


Figure 3.3: Prototype using GEM foils glued to GRP (glass-fiber reinforced plastic) and glass frames. The electrical shielding has been removed. The entrance window for neutrons is at the bottom side and not visible.

CASCADE detector does not require any precious counting gases as discussed in section 2.3.

Figure 3.3 shows an early prototype based on the frame concept. Its electrical shielding has been removed to make the components visible. The stack of frames is mounted on a base plate made of aluminium which also carries parts of the electronics and connectors. This detector was tested at the PSI and is described in more detail in chapter 4.

3.1.1 Material Selection for Neutron Detectors

Interactions of Neutrons with Matter

Neutrons do not carry an electric charge and can therefore only interact with the electrons of atoms via their magnetic dipole moment or weak interactions. The dominant interactions with matter are therefore scattering and absorption by nuclei,

element	σ_c [barn]	σ_i [barn]	σ_s [barn]	σ_a [barn]
H	1.7568(10)	80.26(6)	82.02(6)	0.3326(7)
^{10}B	0.144(8)	3.0(4)	3.1(4)	3835.(9.)
^{11}B	5.56(7)	0.21(7)	5.77(10)	0.0055(33)
C	5.550(2)	0.001(4)	5.551(3)	0.00350(7)
N	11.01(2)	0.50(12)	11.51(11)	1.90(3)
F	4.017(14)	0.0008(2)	4.018(14)	0.0096(5)
Al	1.495(4)	0.0082(6)	1.503(4)	0.231(3)
Si	2.1633(10)	0.004(8)	2.167(8)	0.171(3)
Fe	11.22(5)	0.40(11)	11.62(10)	2.56(3)
Cu	7.485(8)	0.55(3)	8.03(3)	3.78(2)

Table 3.1: Cross sections between thermal neutrons ($\lambda = 1.8 \text{ \AA}$) and a selection of elements in their natural isotope composition. σ_c , σ_i and σ_s are the coherent, incoherent and total scattering cross sections, respectively, σ_a is the cross section for absorption. [Neu92]

which are caused by the strong force.

Coherent and incoherent scattering processes are distinguished amongst scattering processes for neutrons. Coherent scattering means that there is a fixed phase relation between all partial waves scattered by a sample and constructive interference may lead to Bragg peaks. Differences in the scattering behaviour of different isotopes and varying spin orientations of the scattering nuclei may cause incoherent scattering of the sample as a whole.

Absorption processes include all interactions where neutrons are captured by a nucleus, i. e. radiative neutron capture (n, γ), decay processes (n, α), (n, β) and (n, p) and fission (n, f).

The cross sections for absorption σ_a and the cross section for incoherent scattering σ_s both depend heavily upon the neutron energy. From a classical point of view, they scale with the interaction time t of the neutron and the nucleus:

$$\sigma \propto t \propto \frac{1}{v} \quad \Rightarrow \quad \sigma = \frac{v_0}{v} \sigma_0 = \frac{\lambda}{\lambda_0} \sigma_0,$$

where σ_0 is the cross section for thermal neutrons of wave length $\lambda_0 = 1.8 \text{ \AA}$ or $v_0 = h/(m_N \lambda_0) \approx 2200 \text{ m s}^{-1}$.

Table 3.1 displays cross sections for coherent and incoherent scattering and absorption. These cross sections vary significantly between different elements and isotopes.

Material Selection

Different parts of the CASCADE detector impose different restrictions on the attributes of the materials used to build them. Three different components can be distinguished:

1. the sensitive neutron detection area
2. frames that carry GEM-foils, the drift electrode and the readout structure
3. the backside of the detector, which carries various connectors for power and gas supply, signal readout and parts of the readout electronics.

Neutron Sensitive Area

The restrictions on the choice of material for the sensitive area are very tight. Apart from the neutron conversion layers made of ^{10}B , all other materials employed should not interact with the incident neutrons. Yet, absorption is tolerable as it only decreases the number of detectable neutrons by the CASCADE detector and leads to a reduced detection efficiency. Thermal and cold neutrons scattered incoherently are emitted into 4π as this is a s-wave only scattering process. The fraction of the latter consequently limits detection dynamics of the detector and degrades the position information of any event considerably. The dynamics is defined as the maximum ratio between the count rate of two adjacent readout channels and is a measure of the maximum contrast obtainable.

As a consequence, hydrogen in particular and any other material with a large cross section for incoherent scattering, have to be avoided. This certainly comprises any material that contains hydrogen, such as plastics or other organic materials. GEM-foils, the basis of the CASCADE detector, consist of Kapton and copper. They have been tested for their suitability for neutron detectors as part of this diploma thesis and the results are shown in section 3.1.2. These experiments suggest that other materials might be preferable to Kapton. Future developments on this subject are planned.

Frames

The choice of material for the frames is much less problematic. They need not be irradiated by the neutron beam incident on the detector. This is achieved by shielding with neutron absorbing materials. Since neutron beams are always divergent, any hydrogen content should be kept to an absolute minimum.

Currently, the frames are either made of insulators like GRP and glass or of metals like aluminium or stainless steel. Insulators automatically provide the insulation between two adjacent GEM-foils, whereas metal frames implicate the need for additional insulation layers. GRP frames are simple to produce and handle. Due to their hydrogen content they are not considered suitable for the final design of the

CASCADE detector. Silica glass promised to solve this problem, but the glass frames have proved to be sensitive to damage.

Detectors covering large areas of up to $30 \times 30 \text{ cm}^2$ are only possible when using metal frames. If shaped in a special way, these frames will provide the necessary tension to stretch the GEM-foils glued onto them. This prevents sagging of the foils and ensures a constant distance between the GEMs.

Since the depth of the frames does not have to be increased notably for larger frames, detectors using larger frames have a better ratio between the size of the sensitive area and the size of the complete detector including the frames.

The adhesives used to glue the GEM-foils onto the frames always contain large portions of hydrogen [Bru02]. Hence, their usage should be reduced to a minimum. Indeed detector tests have shown that the frame area scatters neutrons considerably if irradiated by neutrons.

Backside of the Detector

For the backside of the detector materials of any kind can be used. This part of the detector is shielded from the neutrons by a neutron absorbing material like cadmium (Cd), gadolinium (Gd) or a thick layer of boron (^{10}B). An additional absorber for gamma particles emitted by the neutron absorbers might prove necessary to protect the readout electronics.

3.1.2 Material Testing

For a position sensitive detector, like the CASCADE detector, it is vital that incoherent scattering within the detector itself is minimised, as scattering processes which emit into 4π would degrade the positional information of any event detected. Therefore some of the materials used to build the detector were tested at the small angle neutron scattering facility (SANS) at the Paul-Scherrer-Institute (PSI), Switzerland. This facility is described in detail in section 4.1.1.

As of today, GEMs are made of copper-coated Kapton, a polyimide produced by DuPont [DuP02]. Its exact composition is not known to the public. To get an estimate of the usability of Kapton-foils in neutron detectors, the transmission coefficient for neutrons was determined using the 2-dimensional wire chamber at SANS. The sample was placed in front of the detector and irradiated by a monochromatic and collimated neutron beam. The incident neutrons can be scattered, absorbed or transmitted unperturbed by the sample. The transmission coefficient T_{sample} of the sample can be found by comparison of data from the sample and data of the reference.

$$T_{\text{sample}} = \frac{I_{\text{sample}}}{I_{\text{reference}}},$$

provided that the incident neutron intensity does not vary. I denotes the intensity as detected, which was normalised to the integrated counts of a beam monitor installed at the beam line to satisfy this condition. A thin aluminium foil was

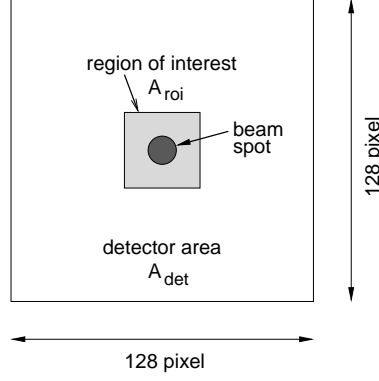


Figure 3.4: Definition of the region of interest (ROI) of the imaging SANS detector. The ROI includes the image of the direct neutron beam.

used as reference sample. According to table 3.1 aluminium is almost completely transparent for neutrons. Only a thin layer of water on its surface scatters neutrons. It is assumed that this layer is the same for all samples and it therefore has no influence on the determination of the transmission coefficient.

The background signal was estimated via the intensity on the outer parts of the position sensitive detector which was not directly irradiated by the beam. This background includes neutrons scattered incoherently by the air between the end of the neutron guide and the entrance window of the SANS detector, background of the hall and neutrons scattered incoherently by water on the surface of the sample. If A_{det} is the sensitive area of the detector and A_{roi} is a region of interest, then the background in the signal on A_{roi} can be estimated as follows:

$$\begin{aligned}
 \langle \text{background in } A_{\text{roi}} \rangle &= \frac{A_{\text{roi}}}{A_{\text{det}}} \cdot \langle \text{background in } A_{\text{det}} \rangle \\
 &= \frac{A_{\text{roi}}}{A_{\text{det}}} \left(\frac{A_{\text{det}}}{A_{\text{det}} - A_{\text{roi}}} \cdot \langle \text{intensity in } A_{\text{det}} - A_{\text{roi}} \rangle \right) \\
 &= \frac{A_{\text{roi}}}{A_{\text{det}} - A_{\text{roi}}} \left(\langle \text{intensity in } A_{\text{det}} \rangle - \langle \text{intensity in } A_{\text{roi}} \rangle \right)
 \end{aligned}$$

The background to signal ratio is $\approx 3 \cdot 10^{-4}$ which is negligible compared to the statistical error of $3 \cdot 10^{-3}$. Therefore, it is not taken into account for further analysis of the data. The error on the transmission coefficient is given by:

$$\frac{\Delta T_{\text{sample}}}{T_{\text{sample}}} = \sqrt{\left(\frac{\Delta I_{\text{sample}}}{I_{\text{sample}}} \right)^2 + \left(\frac{\Delta I_{\text{reference}}}{I_{\text{reference}}} \right)^2}$$

Table 3.2 summarises data and transmission results obtained for two sets of 10 GEM-foils each. The second set had the copper layers removed by etching with

	Aluminium	10 GEM foils	10 GEM foils with copper removed
counts in ROI	259923	123405	124196
counts on detector	263506	125536	126320
beam monitor	32474	17638	17594
Transmission coefficient	1	0.875 ± 0.003	0.882 ± 0.003

Table 3.2: Data on transmission coefficients according to the measurements at the PSI. The area covering the direct beam is denoted region of interest (ROI), $A_{\text{roi}} = 255$ pixels, $A_{\text{det}} = 2^{14}$ pixels.

nitric acid.

$$T = (98.67 \pm 0.03) \% \quad \text{for a single GEM-foil}$$

$$T = (98.75 \pm 0.03) \% \quad \text{for a single GEM-foil without copper layers}$$

This means that losses for a single GEM-foil are limited to 1.33%. Removal of the copper layers leads to a minor improvement of the transmission coefficient by 0.08%. This clearly shows that the losses in the GEM-foils are mostly due to the Kapton itself. They are most likely to be attributed to the hydrogen content in the Kapton. The calculated transmission coefficient includes unperturbed transmission as well as small angle scattering. Based on these measurements these contributions cannot be distinguished.

Incoherent Scattering

The fraction of neutrons that are not included in the transmission coefficient derived in the last section, are either absorbed or scattered incoherently. The percentage of incoherently scattered neutrons S_{is} can be derived by subtracting the integrated intensity of the aluminium reference measurement from the integrated intensity of the sample as follows:

$$\begin{aligned} I_{sc} &= \langle \text{intensity of scattered neutrons in } (A_{\text{det}} - A_{\text{roi}}) \rangle \\ &= \langle \text{intensity in } (A_{\text{det}} - A_{\text{roi}}) \text{ of sample} \rangle - \\ &\quad \langle \text{intensity in } (A_{\text{det}} - A_{\text{roi}}) \text{ of reference} \rangle \\ &= I_s - I_r \end{aligned}$$

This intensity has to be normalised to the area of the sphere which is covered by the SANS detector and the incoming intensity:

$$\begin{aligned} S_{is} &= \frac{A_{\text{det}} - A_{\text{roi}}}{4\pi d^2} \frac{\langle \text{intensity of scattered neutrons in } (A_{\text{det}} - A_{\text{roi}}) \rangle}{\langle \text{incoming intensity} \rangle} \\ &= \frac{A_{\text{det}} - A_{\text{roi}}}{4\pi d^2} \frac{I_{sc}}{I_0} = \frac{A_{\text{det}} - A_{\text{roi}}}{4\pi d^2} \frac{I_s - I_r}{I_0}, \end{aligned} \tag{3.1}$$

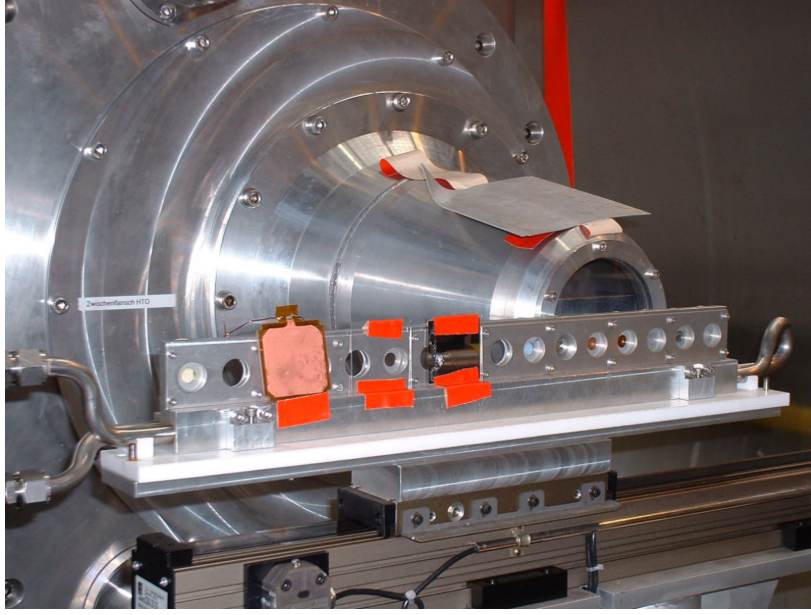


Figure 3.5: Sample holder for the transmission and scattering experiments at the SANS instrument in front of the entrance window of the 20 m long evacuated neutron flight tube.

where d is the distance from the sample to the detector. The statistical error is given by:

$$\Delta S_{is} \approx \frac{A_{\text{det}} - A_{\text{roi}} \sqrt{I_s + I_r}}{4\pi d^2} \frac{1}{I_0} \quad (3.2)$$

The application of equations 3.1 and 3.2 to the measurements at the PSI did not lead to significant results. This was due to very poor statistics and large background noise. Future measurements should increase statistics with neutron beams of higher intensity and extended measurement periods. Figure 3.5 shows the sample holder of the experiment described above as supplied by the SANS responsible. The entrance window of the flight tube (see figure 4.1) was not completely covered by the sample holder. This allowed neutrons, scattered incoherently by the air between the end of the neutron guide and the sample holder to enter the flight tube. These scattered neutrons are the reason for a large background in the scattering signal. A proper shielding of the entrance window could easily avoid this and make future measurements more sensitive and accurate.

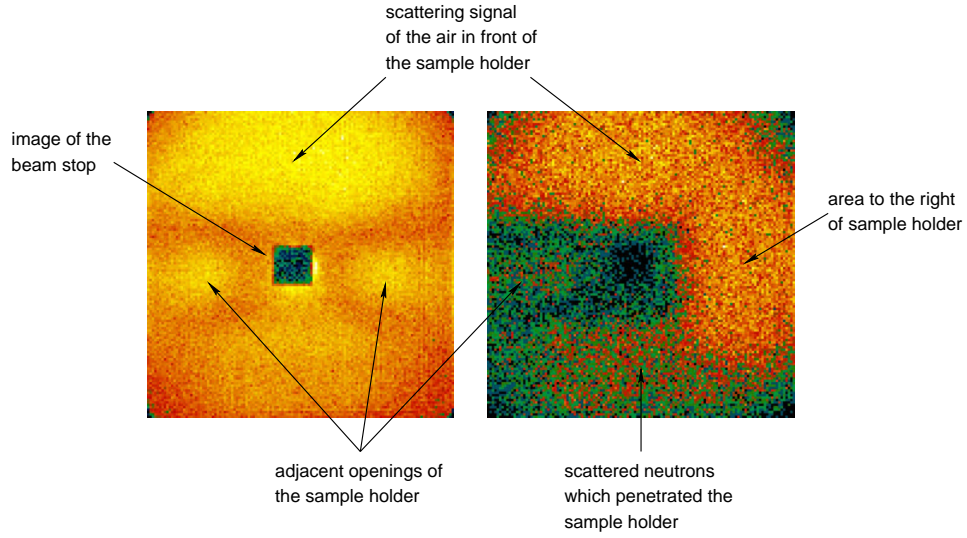


Figure 3.6: Images taken by the 2d SANS detector for a sample (left) and a cadmium absorber (right). The sample holder shown in figure 3.5 was used. The black rectangular area in the middle is shielded from the neutrons by a beam stop.

Conclusion

The area density equivalent D for hydrogen in the GEM-foils can be calculated according to

$$T = \exp\left(-D \frac{\sigma_H(\lambda)}{m_H}\right), \quad \sigma_H(\lambda) = \frac{\lambda}{\lambda_0}(\sigma_{H,a} + \sigma_{H,i}), \quad (3.3)$$

where T is the neutron transmission coefficient as discussed above, σ_H the combined cross section of incoherent neutron scattering $\sigma_{H,i}$ and neutron absorption $\sigma_{H,a}$ by hydrogen, $m_H = 1.673 \cdot 10^{-27}$ kg is the mass of a hydrogen atom and $\lambda_0 = 1.8 \text{ \AA}$ is the wave length of thermal neutrons. Solving the equation 3.3 for D yields

$$D = -\frac{m_H}{\sigma_H} \ln T, \quad \Delta D = \frac{m_H}{\sigma_H} \frac{\Delta T}{T}$$

Substituting $\sigma_{H,i} = 80.59$ barn, $\sigma_{H,a} = 0.332$ barn, $T = 0.9875(3)$ and $\lambda = 8 \text{ \AA}$ results in

$$D = 5.8(4) \cdot 10^{-4} \frac{\text{kg}}{\text{m}^2}.$$

This may be partially attributed to water on the surface of the GEM-foils as the reference for this measurement consisted of a single aluminium foil whereas the sample was a stack of ten GEM foils. The hydrogen content in the Kapton limits

the maximum contrast obtainable by the CASCADE detector. In the future, Kapton may therefore be replaced by other materials which scatter neutrons less.

Scattering experiments at the SANS instrument currently require careful measurements of reference samples. Beam monitors installed along the beam line have to be used to match the number of incident neutrons on the sample between measurements of the sample and the reference. This introduces large uncertainties. Direct measurements of the number of neutrons which penetrated the sample unperturbed would be desirable. They could be used to normalise the scattering measurements and could thereby eliminate the need for reference measurements.

These measurements are impossible with the current setup of the SANS instrument because the direct neutron beam would saturate the SANS detector. Therefore, the beam is absorbed completely by a beam stop. Section 4.1.1 describes the SANS instrument in more detail and presents a solution to this problem, namely the CASCADE beam monitor.

3.2 Electronics and Software

The demands on the CASCADE detector concerning its infrastructure are much higher than those of e. g. single ^3He counter tubes. A CASCADE module in its final stage (as planned today) will contain 10 GEM-foils in a symmetrical setup. This means that neutrons will be exposed to a total of 20 boron layers. It will have an active area of 30 cm by 30 cm and will offer 10^4 pixels combined in 200 readout channels, 100 for every dimension. Each channel will be capable of event rates on the order of 10^6 s^{-1} . Moreover, several of these detector modules may be used together to cover large areas. This leads to challenging demands on the readout electronics which are yet unknown in neutron physics. The technical solutions to such challenges have been found in high energy physics. The following sections describe the infrastructure for the signal readout and the way it was transferred from high energy physics to the neutron sector for the CASCADE detector.

3.2.1 The New Hardware Concept

The transfer of technology and hardware developed for high energy physics makes advanced and reliable electronics available for the CASCADE detector. It will form the basis of the readout electronics. Future developments will take care of an even better adaption to the needs of the CASCADE detector. Figure 3.7 gives an overview of the infrastructure.

The central and most important element of the electronics is the processing of the readout signals. The primary processing of the detector signals will be done by an integrated circuit, the CIPix chip. This chip integrates many readout channels using very little space. Its functionality is described in the next section.

The CIPix chip is complemented by electronics to program the chip as well as electronics for further processing of its digital output signals. The latter is done

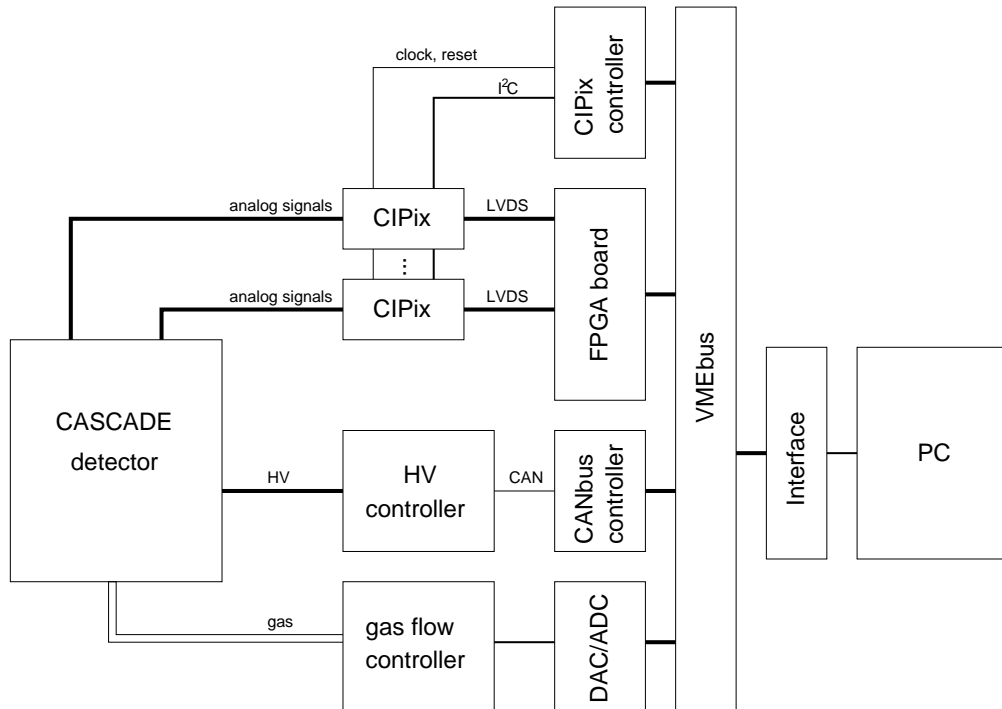


Figure 3.7: Sketch of the detector infrastructure

by programmable electronics through FPGA¹ technology. It will be configured to make primary trigger decisions, to sum up event counts and to compress event data, depending on the actual application of the CASCADE detector.

The detector is completely controlled via the VMEbus. This bus has proven its reliability as an industrial standard for years and plenty of modules are readily available, e. g. the DL535 summing board described in section 3.2.3 [EW]. Currently, a PCI² to VMEbus interface by WIENER [Wie] connects the detector system to a standard PC. Should the demand on data throughput increase, it will eventually be replaced by a VME PC module.

Up to 16 high voltage channels are provided by the iseg EHQ F025 power supply [Ise]. This appliance was developed for the ATLAS project. The output voltage of every single channel can be controlled and monitored independently via a CAN bus interface. A VMODFCAN CAN bus controller by Janz [Jan] connects the power supply to the VMEbus.

The gas supply is implemented using standard gas flow controllers, one for every component of the counting gas. These are driven by analog signals provided by DL629 DAC VMEbus modules. The actual gas flow is also monitored by DL626 ADC VMEbus modules [EW].

¹Field Programmable Gate Array

²Peripheral Component Interconnect

The electronics described above replace a huge variety of systems, such as CAMAC based readout electronics, PCI cards built into the PC and several NIM modules. These systems were controlled via an even greater variety of interfaces. The control over the electronics was simplified by the introduction of a single interface between the PC and the rest of the hardware: the VMEbus. As part of this thesis almost all of the electronics were replaced. An extendible software library was developed which allows easy access to the features provided by the new hardware. This library is described in section 3.2.4.

3.2.2 The CIPix Chip

CIPix is an ASIC³ chip developed by S. Löchner [Löc98] and D. Baumeister [Bau99] at the ASIC-laboratory of the University of Heidelberg. It was originally intended to be the readout chip for the proportional chamber of the inner tracker system of H1 at the storage ring facility HERA. The CIPix was derived from the HELIX128 chip, which is used for the inner tracker system of HERA-B at DESY. It contains the same analogue front end developed by U. Trunk.

This ASIC integrates 64 analogue readout channels, each of which consists of a low-noise preamplifier, a shaper, a buffer amplifier and a discriminator. The digital discriminator signals are generated synchronously to a clock of 10 MHz. They are then combined into 16 signals plus a synchronisation signal by a time-division multiplexer. All necessary reference voltages and currents are generated internally and can be programmed via an I²C-interface. An internal test pulse generator facilitates testing of the chip as well as of its carrier board.

Figure 3.8 shows a block diagram of the CIPix 1.1 chip internals. The charge sensitive preamplifier has a gain of $\approx 40 \text{ mV} / 10^5 \text{ electrons} = 2.5 \text{ mV} / \text{fC}$. Its noise level depends linearly on the capacity at the input. Measurements yielded a noise level of $380 e^- + 38 e^- / \text{pF}$ [Bau99]. The shaper forms an asymmetric pulse with a longer tail and a peak time in the range of 50 to 70 ns, again depending on the capacity at the input. A complete description of the technical details of this chip can be found in [Löc98], [Bau99], [Sta00] and [Sch02].

Figure 3.9 shows the CIPix-chip bonded to the current test board. These boards are controlled by a DL641 submodule, which is a mezzanine board mounted on a DL600 VMEbus module. This system was developed by A. Rausch at the electronics workshop of the Physics Institute [EW]. It provides the necessary clock signals (10 MHz and 40 MHz), the required reset logic (hard- and soft-reset) and offers an I²C-interface to support and control several CIPix-modules.

These test boards are currently evaluated. Several modules have already been programmed via the I²C bus and the characteristics of the analogue front end of the CIPix are analysed. Next to come are real life tests of the CIPix as readout system of the CASCADE neutron detector.

³Application Specific Integrated Circuit

3.2.3 FPGA Board

The multiplexed digital output of the CIPix-chip is connected to a FPGA via a LVDS⁴ link as depicted in figure 3.7. The FPGA is mounted to a DL541 VMEbus board. This board was initially designed as a summing board for the H1 CIP2000 upgrade project. It features a powerful FPGA (Apex EP20K400 [Alt]) which contains about $4 \cdot 10^5$ gates and facilitates complex processing tasks.

The FPGA code will include a demultiplexer for the multiplexed data from the CIPix, the trigger logic, counters or buffers for the event data and the VMEbus interface logic. Depending on the actual application of the CASCADE detector the flexibility of the FPGA can be used to implement custom tailored electronics without changing the hardware. The generation of time stamps for time-of-flight measurements is one example for this. Moreover, this board may detect multiple, simultaneous events and reject them. This might be necessary for 2-dimensional readout structures which are not based on single pads, but rather use stripes in x- and y-direction to reduce the number of channels. In this case, the coordinates of multiple events cannot be determined in a non-ambiguous way.

3.2.4 Hardware Access Library

To simplify access to the new hardware described in the previous sections, an efficient and easy to use software library had to be developed. An object-orientated approach has been taken to map hardware modules, bus-types and interfaces to object classes offering a layer of abstraction over the pure hardware access.

The implementation was done using C++ under the Windows operating system, being the common standard of the working group at the moment. The portability was not one of the major goals of the development, although care was taken to ensure portability to other operating systems and different VMEbus interfaces and drivers.

The usage of an object oriented language introduces a slight run-time overhead compared to procedural languages like C. Modern highly optimising compilers help to minimise this effect. Speed comparisons between C++ and C code have not shown any measurable effect on VMEbus access times via the PCI to VME interface by WIENER .

The next section will describe the major design principles of the library. As the complete source code comprises about 5000 lines of code, it is not included here.

Implementation Details

Error detection and handling is an essential part of this library. Therefore all classes directly or indirectly inherit from the `ErrorLib`⁵ class, which offers a generic interface to error handling and error message retrieval. It serves as the root of the inheritance tree which can be seen in figure 3.10.

⁴Low Voltage Differential Signaling

⁵always add a C prefix to get the actual class names

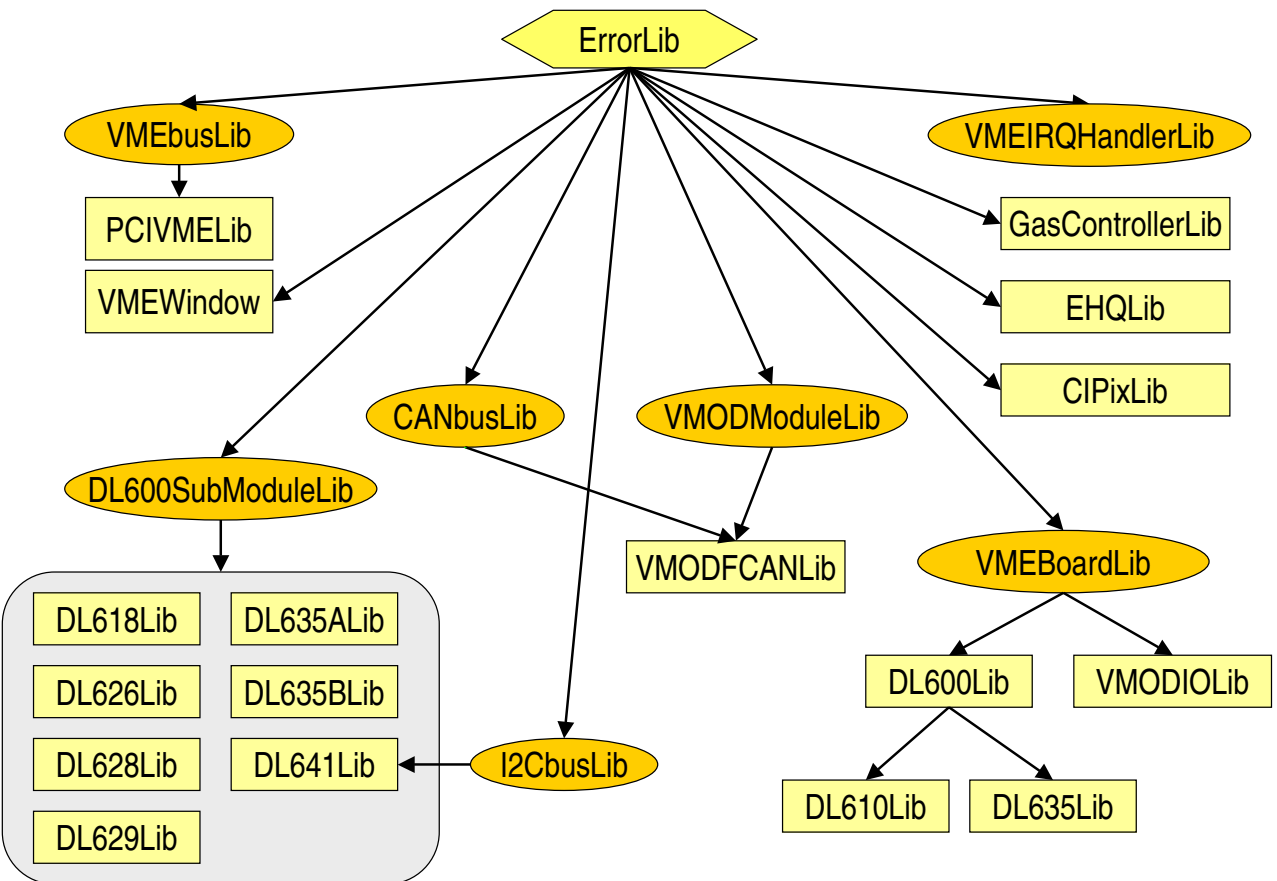


Figure 3.10: Inheritance tree of the hardware access library, black arrows denote inheritance, abstract classes are represented by ellipses, normal classes by squares

The library defines several abstract classes that are not meant for instantiation but rather define common interfaces, methods and data fields. The `CANbusLib`, `VMEBusLib` and `I2CbusLib` classes for example provide common methods and interfaces for the access of different bus systems while retaining hardware independence. Different hardware implementations are represented by classes which are derived from these virtual base classes. This allows for polymorphism⁶ to be used and ensures that different classes representing different hardware implementations may be used interchangeably.

Description of the Library Classes

ErrorLib is the root class from which all other classes are derived directly or indirectly. It offers a common interface to error codes and error message retrieval. Derived classes inherit virtually from this class to ensure that only one copy of the object—including data and interfaces—is stored in any derived class in the case of multiple inheritance.

VMELib abstracts the interface to the VMEbus. It defines methods for read and write access, interrupt handling and registration of VMEbus boards. Specialised methods for block transfers and transfers from FIFO buffers are available.

PCIVMELib inherits from `VMELib`. It is the actual implementation for the Windows 9x driver of the WIENER PCIVME interface that is used as a PCI to VME bridge at the moment. It uses the class `VMEWindow` internally, which is of no direct use to the user. `PCIVMELib` is the only class that is dependent on PC hardware and drivers. It is therefore the only class which has to be replaced by another driver and hardware specific implementation for operating systems like Linux and Windows NT etc., or other hardware interfaces.

VMEBoardLib defines a generalised interface to boards on the VMEbus. All instances of `VMEBoardLib` or its descendants, respectively, automatically register with a given instance of `VMELib`. This simplifies the handling of external bus resets and initialisation of all boards.

DL600Lib derives from `VMEBoardLib`. It represents the mezzanine module carrier board DL600 developed by the electronics workshop of the Physics Institute [EW] and handles all functionality common to all submodules. This board may carry up to four submodules of various types and functionalities. The `DL635Lib` e.g. is derived from this class and represents a DL600 board equipped with one DL635A and three DL635B submodules to build an array of 11 synchronous counters.

⁶In object-oriented programming, polymorphism (from the Greek meaning *having multiple forms*) is the characteristic of being able to assign a different meaning or usage to something in different contexts - specifically, to allow an entity such as a variable, a function, or an object to have more than one form.”[definition found at www.what-is.com]

DL600SubmoduleLib is designed to be the base class for all DL600 mezzanine boards representations. It implements some methods common to all sub-modules and automatically registers the instance with its carrier board class instance.

Plenty of classes derive from **DL600SubmoduleLib** as can be seen in figure 3.10. The following table gives a brief description of all subclasses implemented at the moment:

DL618Lib	RS232 interface
DL626Lib	ADC module with 8 input channels
DL629Lib	DAC module with 8 output channels
DL635ALib	counter module and control unit with 2 counters
DL635BLib	counter module with 3 counters
DL641Lib	CIPix control module (clocks and I ² C interface)

VMEIRQHandler abstracts the interface for interrupts generated on the VMEbus. At the moment none of the hardware in use depends on interrupts, so that no class inherits from it. It has been added for completeness and future extensions.

CANbusLib abstracts the interface to the CANbus. It is an abstract class which only defines an interface for the bus access. The **VMODFCANLib** implements this interface for the VMOD-FCAN module from Janz Automationsysteme AG [Jan97b]. This is a mezzanine board for the VMOD-IO card which is represented by the **VMODIOLib** class [Jan97a].

I2CbusLib offers an abstract interface to the I²C bus. The I²C bus is a two wire serial bus and defined in [Phi95] and [Phi00]. The current implementation of this class supports the 10 bit addressing scheme and is limited to interfaces which give direct access to both lines of the bus.

CIPixLib serves to abstract the interface to the CIPix chip. The internal registers of the chip are controlled via a **I2CbusLib** interface class. Methods for hard- and soft-resets of the chip are provided.

EHQLib is the software representation of the high voltage supply EHQ. Several methods give access to a broad subset of the functionality of this device, including voltage control and monitoring. Commands are sent to the device via an implementation of **CANbusLib**.

GasControllerLib controls one of the gas flow controllers via an instance of **DL629Lib**. Monitoring of the actual gas flow is done via an instance of **DL626Lib**.

4 Detector Prototypes and Measurements

This chapter gives a detailed description on prototypes of the CASCADE detector, which were built as part of this thesis. Details of the construction as well as the demands on these prototypes can be found in section 4.1. Their main characteristics, namely neutron detection efficiency, spatial resolution and rate capability were tested at the PSI and the ILL. Section 4.2 describes these measurements. As a first application, time-of-flight (TOF) measurements were performed at the beamline PF1A at the ILL. These measurements are described in section 4.3. They clearly show the enormous advantages of the CASCADE detector over conventional detectors.

4.1 Detector Prototypes

4.1.1 The Beam Monitor for SANS at the PSI

During the tests of the CASCADE detector at the Paul-Scherrer-Institut, Switzerland (PSI) which took place prior to this work, it became evident that a beam monitor for the direct neutron beam would be of great benefit for the Small Angle Neutron Scattering facility (SANS).

The requirements on this beam monitor were defined in discussions with the instrument responsible J. Kohlbrecher as part of this diploma thesis. The monitor was then designed, built and tested successfully in accordance to these technical demands.

The following sections describe the SANS instrument itself as well as the CASCADE beam monitor built for this instrument.

The Small Angle Scattering Facility at the PSI

The SANS instrument at the PSI is a typical small angle neutron scattering facility. A sketch of its layout can be seen in figure 4.1. Its main purpose is to measure the coherent scattering signal from a sample. Its 2-dimensional neutron detector is a position sensitive ^3He -wire chamber with 128×128 elements of $7.5 \times 7.5 \text{ mm}^2$. The detector is located in a 20 m long evacuated flight tube and is laterally displaceable within the tube. By repositioning the detector along the tube, the angular resolution can be adjusted to the desired value. Samples are placed in front of the flight

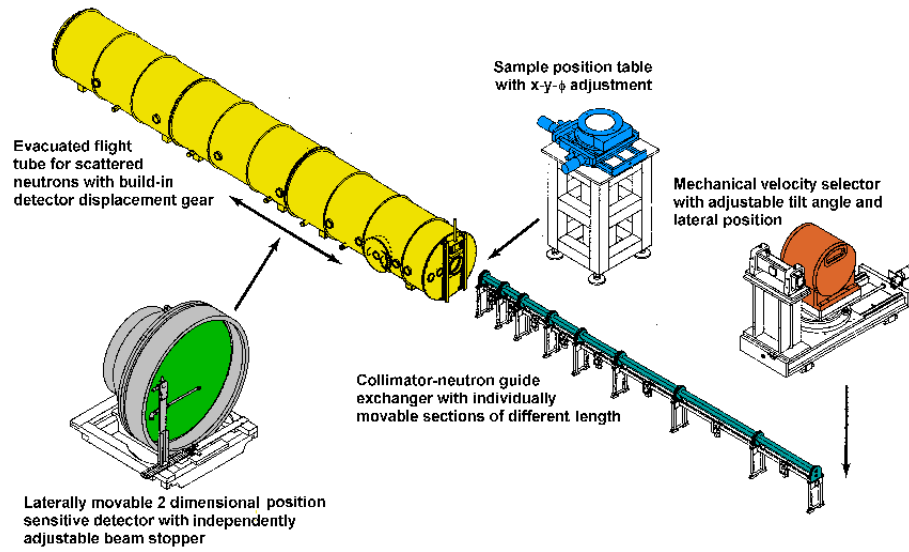


Figure 4.1: Main components of the small angle neutron scattering facility at the PSI [SAN02]

tube and irradiated with an intense neutron beam. A collimation system allows collimation lengths ranging from 1 m to 18 m. Different apertures may be inserted into the neutron beam to reduce its intensity. A helical-slot velocity selector with adjustable rotation speed is used as monochromator with a resolution of $\Delta\lambda/\lambda \approx 10\%$ (FWHM). The neutron spectrum at the SANS site can be seen in figure 4.2. It has a wave length range of $0.45 \text{ nm} < \lambda < 4 \text{ nm}$.

Neutrons are generated in the Swiss Spallation Neutron Source (Spallationsneutronenquelle, SINQ). This is a continuous source with a total flux of about $10^{14} \text{ cm}^{-2} \text{ s}^{-1}$. Neutrons are emitted by spallation processes of a lead target which is irradiated by a pulsed proton beam of about 1.3 mA at an energy of 570 MeV. The neutrons are then moderated by heavy water. This moderator forms the source for thermal neutrons. Further moderation by liquid deuterium at 25 K cools the neutrons further down for the cold neutron source. This source is used for the SANS instrument.

The neutrons are transported to the SANS instrument—and to other experiments—with the help of neutron guides. Figure 4.2 shows the neutron flux at the specimen position of the SANS instrument as a function of the neutron wave length. It is linearly dependent on the proton current.

Samples normally scatter only a small fraction of the incident neutrons. The rest is either absorbed or transmitted unperturbed. At a proton current of 2 mA the neutron flux will be as high as $10^7 \text{ s}^{-1} \text{ cm}^{-2}$. In the current setup of the instrument the unperturbed fraction of the neutron beam is absorbed completely by a beam

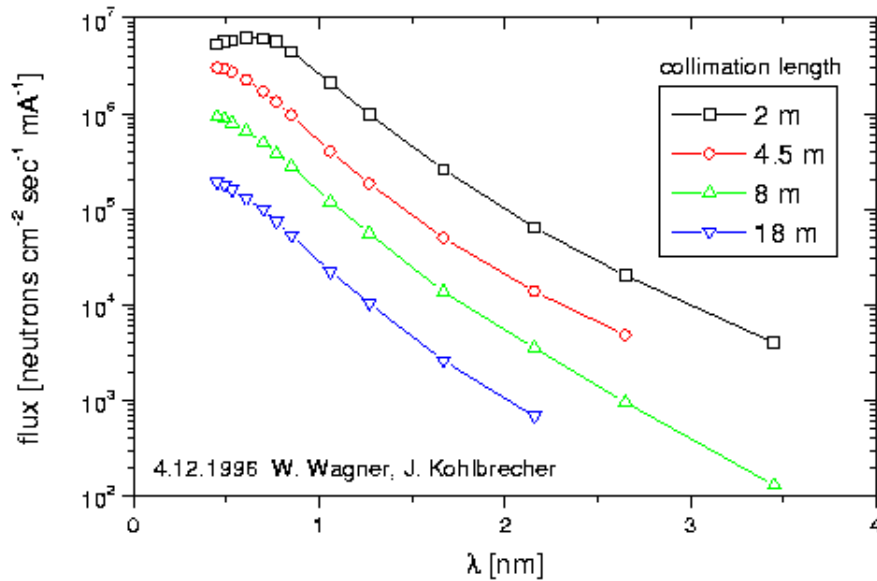


Figure 4.2: Neutron flux at the sample position of the SANS instrument. Results were obtained by activation measurements of a gold foil. The flux is linearly dependent on the proton current of the SINQ. [SAN02]

stop. It is mounted on a movable aluminium arm which is positioned directly in front of the 2d detector. Measurements of the direct beam are impossible because they would saturate the ^3He wire chamber detector. These would be desirable, however.

Along the beamline several beam monitors are installed. They monitor the proton current of the SINQ, the intensity of the ‘white’ and the monochromatic neutron beam. These monitors can be used to normalise all count rates of the SANS detector to some measure of the incident neutron flux. However, none of these monitors can entirely replace a monitor for the direct neutron beam. The CASCADE beam monitor described here will complete the setup. It is designed to be placed in front of the current beam stop where it will detect the neutrons which penetrated the sample unperturbed, eliminating the need for reference measurements to normalise the data.

Design of the Beam Monitor

In order to minimise the changes to the SANS instrument several conditions had to be taken into account. These requirements have been extracted from several discussions with the responsible of SANS instrument, J. Kohlbrecher, and technicians of the PSI:

- The location of the beam monitor in front of the 2-dimensional wire chamber necessitates that no incoherent scattering of neutrons is caused by any materials which were used for its construction. This is especially true for the high voltage ‘cable’ and the signal readout connection as those have to be positioned in front of the detector (see figure 4.1).
- The detector must be absolutely gastight as it will be placed into a vacuum of about 10^{-2} mbar. A constant gas flow through the detector is currently not possible because this would require additional gas pipes in front of the 2d detector. These would increase damping and scattering of the neutrons, which were scattered by the sample. Additionally, a mechanical feed through for the gas supply would be necessary.
- The preamplifier for the readout signal cannot be placed on the backside of the beam monitor because this would require additional cabling. The amplifier would have to be placed in the vacuum, which could lead to overheating.
- The active area of the detector should be quadratic with a width of 40 to 50 mm. The width of the housing must not exceed 75 mm and its depth must be smaller than 80 mm.

This meant that the SANS beam monitor had to differ considerably from all other prototypes (e. g. those described in section 4.1.2 and 4.1.3). The result can be seen in figure 4.3, which shows the interior of the detector.

The gastight housing is made out of aluminium and sealed by an O-ring. The drawings for the housing can be found in appendix B. The two feed-throughs for the high voltage and the readout signal are made of tungsten and glass. The GEMs are glued to frames. These are made out of glass and are cut out using a water jet. A simple aluminium plate is used as a single pad readout ‘structure’. As a result, the detector is not position sensitive. The drift electrode is an aluminium foil coated with boron.

The detector includes a total of three boron layers: two GEM-foils, which have been coated on the upper side only, and the drift electrode, which is coated on the lower side. The detector stack is completed by a non-coated GEM-foil that is used for signal amplification. The stack is held in place within the housing by 4 threaded bolts, which are screwed to the base plate.

Cabling

A major issue in the design of this detector was the cabling of the high voltage as well as the readout signal. These cables have to be positioned in front of the SANS detector. To ensure that they do not interfere with the SANS measurements, they have to be transparent for neutrons.

As a simplification, the number of voltage cables was reduced to one by the introduction of a potential divider within the detector housing. This was made using standard high voltage resistors which were embedded into a Teflon support.

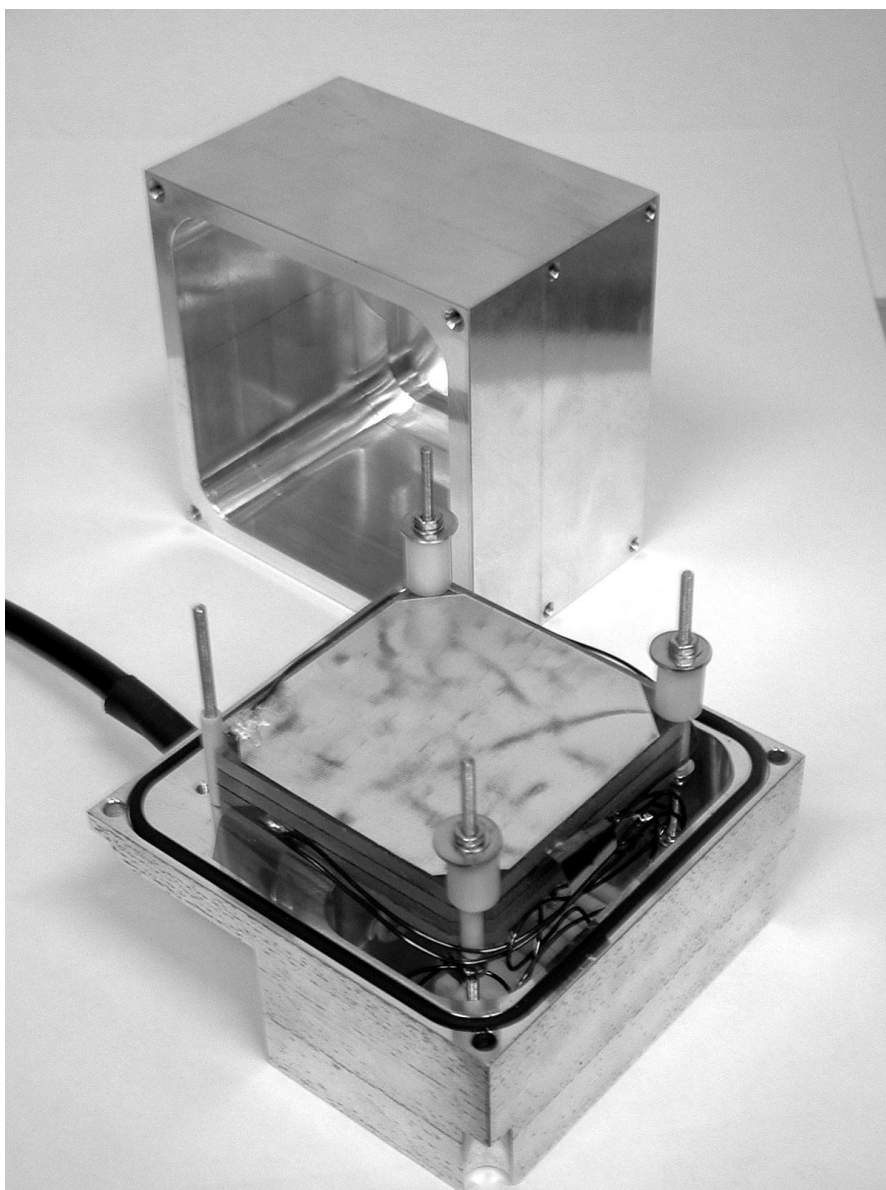


Figure 4.3: The interior of the beam monitor built for the SANS instrument at the PSI. The neutron entrance window is at the top.

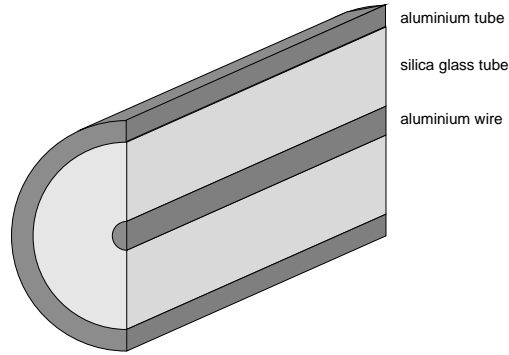


Figure 4.4: Sketch of the neutron transparent coaxial cable.

It provides all 7 voltages needed for the detector stack. The connection to the voltage supply was established by an aluminium cable isolated with a Kapton film. This film is only 25 μm thick and its influence on the neutrons scattered by the sample should therefore be tolerable.

The solution for the readout signal was different. A 70 cm long coaxial cable was built out of an aluminium tube, a fused silica glass tube and an aluminium wire. A sketch is shown in figure 4.4. The characteristic impedance Z_0 of the resulting cable is determined by

$$Z_0 = \sqrt{\frac{L}{C}} = \frac{1}{2\pi} \sqrt{\frac{\mu\mu_0}{\epsilon\epsilon_0}} \ln \frac{b}{a} \approx 60 \sqrt{\frac{\mu}{\epsilon}} \ln \frac{b}{a},$$

where b is the inner diameter of the aluminium tube, a the outer diameter of the wire and μ and ϵ are relative permeability and permittivity of silica glass, which is used as dielectric. The chosen values are $a = 1 \text{ mm}$, $b = 4 \text{ mm}$, $\mu = 1$, $\epsilon = 4.6$, which yields

$$Z_0 = 38.8 \Omega.$$

The input impedance of the preamplifier has been matched to this value. Tests of the detector have shown that there is no significant influence of the long connection between readout structure and preamplifier on the signal to noise ratio.

Results and Conclusions

Due to delays at the PSI this beam monitor has not yet been installed. The installation is planned for the next shutdown period of the SINQ in spring 2003. The detector itself has been tested and its characteristics are outlined in section 4.2.

The signal to noise ratio of this detector is about an order of magnitude. This is comparable to what is achieved by other prototypes which do not use such long readout ‘cables’.

During the tests at the PSI the proton beam of the spallation source¹ was instable.

¹see chapter 3 for a description

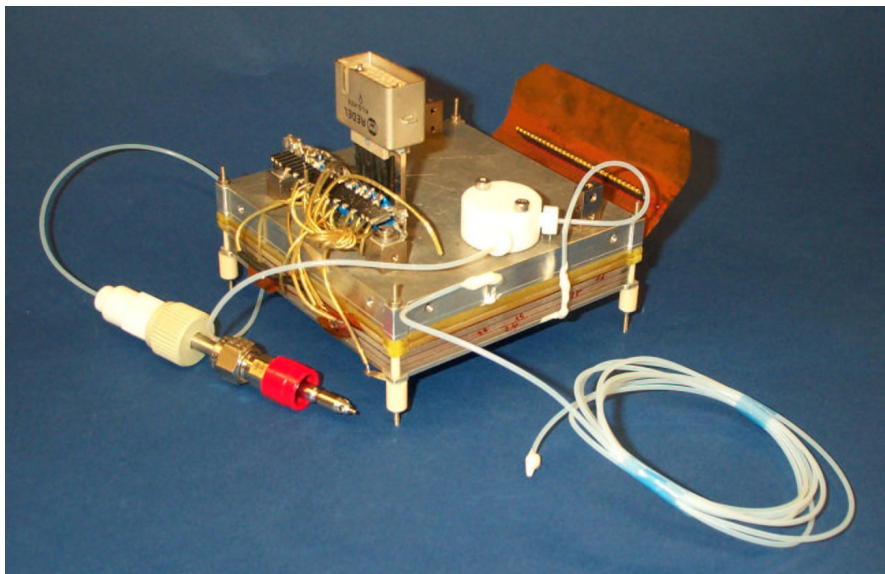


Figure 4.5: Prototype tested at the PSI. The entrance window of the detector is at the bottom side.

The neutron beam did only have a quarter of its normal intensity. Nevertheless the beam monitor already showed its high rate capability. A maximum of 1.13 MHz was detected by the CASCADE beam monitor.

For the first time, glass frames were used to built a CASCADE detector. Glass is a weak neutron scatterer and it is a very good insulator. Glass frames can be easily manufactured using a water jet cutting process. Consequently, it was considered to be an ideal material to be used for the frames. Surprisingly, these glass frames caused intense sparking in the detector. Only the insertion of an extra insulator between every two glass frames inhibited these sparks. The exact cause of this is unclear. The insulators insert surfaces, which are perpendicular to the field lines between the GEMs. Sparks along the rough surface of the glass frames are inhibited. Further tests have to show whether glass frames produced using alternative production processes behave similarly.

4.1.2 PSI Prototype

The PSI prototype—in contrast to the beam monitor described in the last section—was not intended for a permanent installation. It was designed as a test case for the modular design using frames and for the constant flow of cheap counting gases through the detector housing.

The detector stack consists of 2 GEM-foils, each one coated with boron on one side, a non-coated gain-GEM and a boron coated drift electrode made of aluminium. The GEM-foils have an active area of $10 \times 10 \text{ cm}^2$. The frames carrying these foils

were made of insulators: glass and glass-fiber reinforced plastic (GRP). These frames provide electric isolation between the GEM-foils automatically and are easy to manufacture. Clearly the GRP frames will not be used in the final design of the CASCADE detector as their hydrogen content causes a huge deal of scattering of neutrons if exposed to the neutron beam.

The counting gas mixture is provided by an external gas flow controller. The gas connector and pipes made of Teflon can be seen in figure 4.5. The valve to control the gas flow is made of Teflon and mounted onto the base plate.

The readout structure is a simple printed circuit board (PCB) with Kapton as substrate. 33 stripes of a thin gold layer create a one dimensional readout structure. The stripes have a width of 2.8mm and are separated by 0.2mm. For the tests at the PSI, 16 stripes on the left and 16 on the right side of the detector were connected, leaving a single stripe in the middle. Each channel was connected to a VV50 preamplifier. This charge sensitive amplifier was designed by the electronics workshop at the Physics Institute [EW]. It has an integration time of about 200 ns and a gain of about 10 mV fC^{-1} . These amplifiers were mounted onto a circuit board which was attached to the base plate.

A new multi-pin high voltage connector replaces the SHV cabling of previous prototypes. It integrates all necessary power lines into one cable. This system was initially developed for the ATLAS project. The high voltage for the detector was provided by a NHQ205 power supply by iseg [Ise]. The voltages for the GEMs were generated by an A356 controllable voltage divider [EW].

Results

The prototype shown in figure 4.5 was tested at the PSI. The details of these tests can be seen in section 4.2.

The PSI prototype was built as a test case for the modular concept. Initially, its design did not include any electrical shielding. The tests at the PSI approved the functionality of the modular design, yet they clearly showed that proper electromagnetic shielding is a necessity.

This prototype was the first CASCADE detector to measure a count rate exceeding 1 MHz.

4.1.3 ILL Prototypes A and B

The two prototypes tested at the ILL are direct successors to the PSI prototype described in the previous section. One of them can be seen in figure 4.6. They differ from their predecessor only slightly:

- As a result of the experience made at the PSI, the electrical shielding was improved significantly. The detector is completely shielded by an aluminium housing. This housing is made of a 0.5 mm thin aluminium sheet material, which was cut to shape by a laser and was then bent into the correct shape.

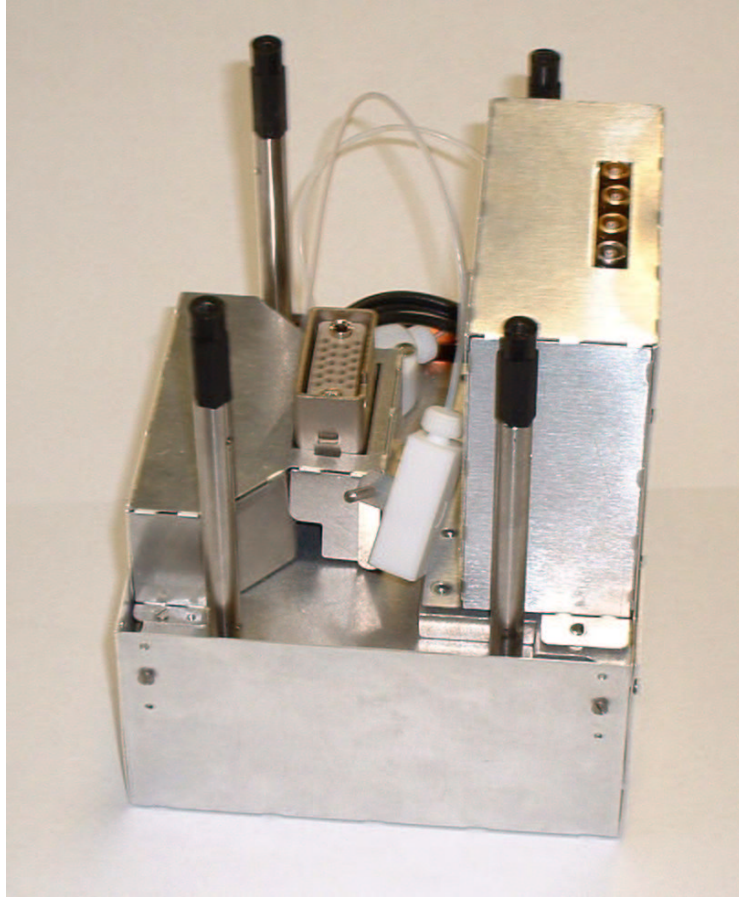


Figure 4.6: CASCADE detector that was tested at the ILL in different configurations

This design provides an efficient shielding against electro-magnetic waves and is very easy to build and attach.

- The readout structure is directly connected to the preamplifiers at the backside of the detector. These preamplifiers are charge sensitive amplifiers with a reduced integration time of ≈ 150 ns. They will be replaced by the CIPix chip in the near future as described in section 3.2.
- Detector assembly was greatly simplified. This makes fast disassembling and reassembling in a different configuration possible. During the tests at the ILL, several different detector configurations were tested.

The first prototype (A) was completely assembled in Heidelberg and remained unchanged during all tests. The second prototype (B) was modified several times. This included opening of the housing, exchange of GEMs and variations of the distance between two GEM-foils.

4.2 Characterisation of the Prototypes

4.2.1 Efficiency Measurements

The total detection efficiency \mathcal{E} of a neutron detector is defined as

$$\mathcal{E} = \frac{\langle \text{number of neutrons detected} \rangle}{\langle \text{number of incoming neutrons} \rangle}.$$

To determine the efficiency the number of incoming neutrons has to be known. This can be achieved by reference measurements, e. g. using a detector with known detection efficiency \mathcal{E}_r and known dead time τ_r or by activation measurements of gold foils.

In the case of the reference detector, the detection efficiency of the test detector can be easily calculated as:

$$\mathcal{E} = \mathcal{E}_r \frac{I_t}{I_r},$$

where I denotes the intensity detected by the test detector or the reference detector, respectively, and \mathcal{E}_r denotes the detection efficiency of the reference detector.

SANS Beam Monitor and PSI Prototype

The SANS beam monitor and the PSI prototype were both tested at the sample position of the SANS instrument at the PSI. A ^3He counter tube provided by the instrument responsible was used as reference. The wave length dependence of the detector efficiency was determined by successive irradiation of both detectors with the same monochromatic neutron beam. Each count rate was normalised to an integrated signal of a beam monitor, which monitored the intensity of the monochromatic beam. This was done to compensate for the varying intensity of

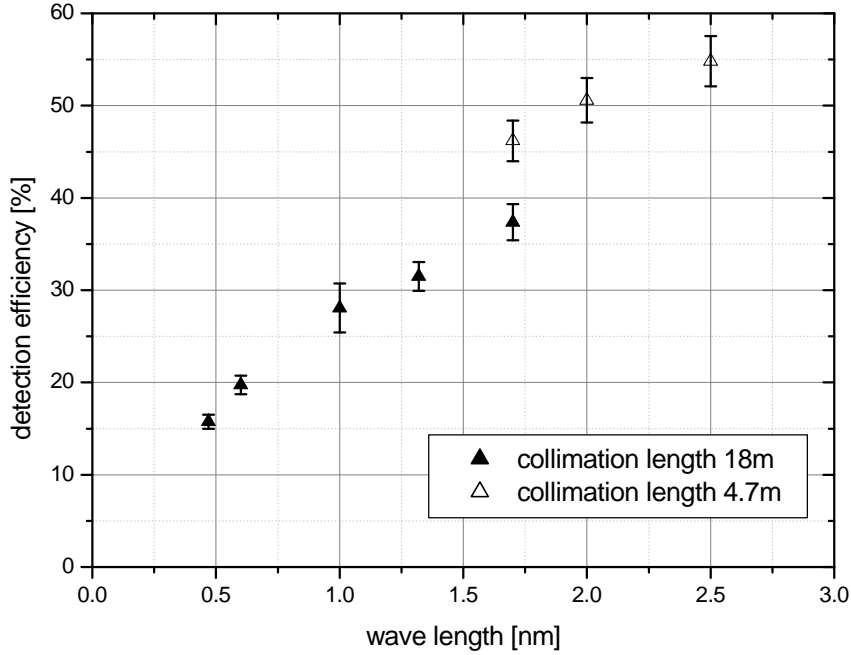


Figure 4.7: Efficiency of the SANS beam monitor. A ^3He counter tube was used as reference. At $\lambda = 1.7$ nm the geometry of the setup was changed.

the neutron beam between the measurements of the test and the reference detector. A dead time correction as described in section 4.2.3 was applied to the intensities measured. The dead time of the reference detector was given to be $\tau_r = 2.4 \mu\text{s}$, the dead time of the CASCADE detector was assumed to be equal to the integration time of the preamplifiers as $\tau = 0.2 \mu\text{s}$. The dead time of the CASCADE detector is dominated by dead time of the readout electronics. The detection efficiency of the ^3He counter tube was $\approx 90\%$ for thermal neutrons ($\lambda = 1.8 \text{ \AA}$).

The error on these measurements has two major contributions: the statistical uncertainty of the count rates and an additional uncertainty of the measurement time due to manual synchronisation between the start of the event counter of the CASCADE detector and the start of the data acquisition of the beam monitors. This uncertainty was $\Delta t \approx 2$ s, which is large compared to the duration of the measurement of 60 s. The wave length resolution of the velocity selector is limited to $\Delta\lambda/\lambda \approx 10\%$ (FWHM).

Figure 4.7 and 4.8 show the resulting wave length dependence on the efficiency of the SANS monitor and the PSI prototype. At $\lambda = 1.7$ nm the intensity of the beam was changed. This was done by removing an aperture which was situated in front of the collimation system on the beamline. Additionally the collimation length was reduced, further increasing the intensity of the neutron beam. Despite this, the

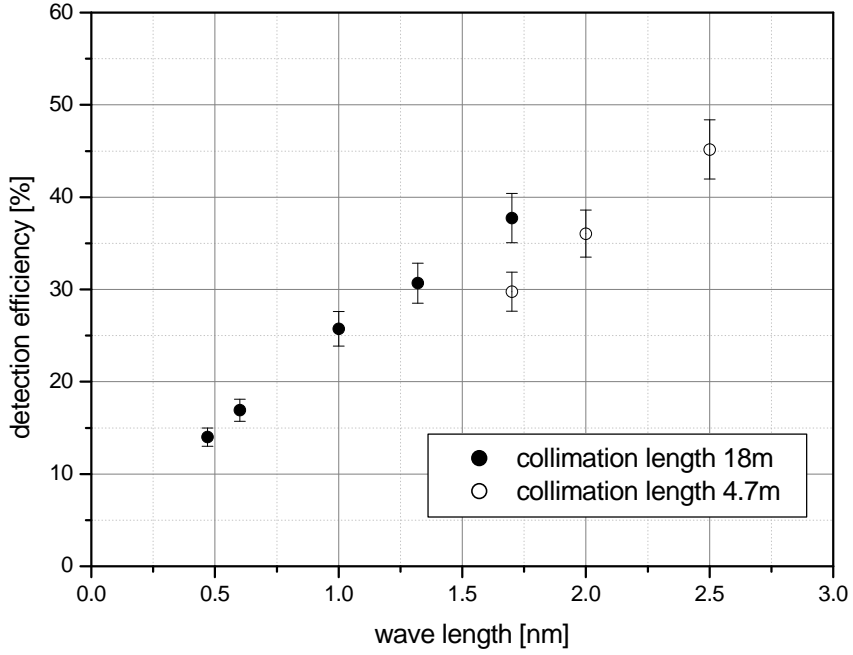


Figure 4.8: Efficiency of the PSI prototype

geometry of the experiment was not changed.

During the analysis of the data it became clear that the changes to the geometry had different effects on the prototypes and the reference detector. The data in figure 4.7 and 4.8 shows a clear step at a wave length of 1.7 nm. This made a meaningful comparison of the measurement results and theoretical predictions impossible.

ILL Prototypes

The CT2 site at the ILL was used to test the prototypes of the CASCADE detector. At this beam site a monochromatic neutron beam is extracted from a polychromatic beam by diffraction off a crystal. Its neutron wave length is $\lambda = 2.5 \text{ \AA}$, which cannot be altered. Therefore only a single measurement concerning the detector efficiency could be made.

The reference counter was a ^3He counter tube provided by the ILL detector workshop. Its detection efficiency was $\mathcal{E}_{ref} = 0.76$ at $\lambda = 2.5 \text{ \AA}$. The test equipment automatically corrected for its dead time. This correction was always kept at a level below 1%.

Dead time of the CASCADE prototype was measured. The results can be seen in the next section. An efficiency of

$$\mathcal{E} = (23.6 \pm 1.1) \% \quad \text{for } \lambda = 2.5 \text{ \AA}$$

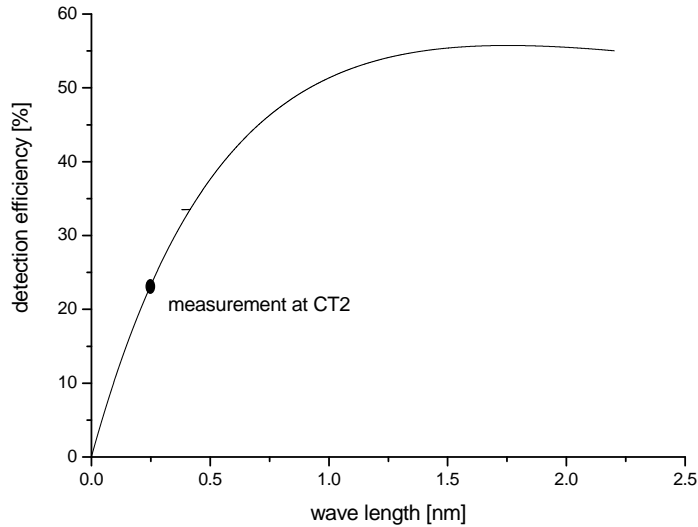


Figure 4.9: Neutron detection efficiency of the ILL prototype A

was determined for the prototype (A), a detector equipped with 8 layers of boron. This measurement is important for a further interpretation of the results of the time-of-flight measurements described in section 4.3.

To determine the wave length dependent detection efficiency of this prototype the thickness of the boron layers was determined independently. The transmission coefficient of ^{10}B layers coated on glass substrates in the same production run as the GEM-foils was measured. Together with the single efficiency measurement at CT2 the loss in the efficiency due to the holes in the GEMs was determined. A result of 35 % loss is in good agreement with the geometrical fraction of area of the holes. These measurements were combined to calculate the detection efficiency as depicted in figure 4.9.

The GEM foils are currently not optimised for neutron detection. The number and size of the holes in the GEM will consequently be altered to match the needs of the CASCADE detector, i. e. the dead area will be reduced to about 5 %.

4.2.2 Spatial Resolution

The spatial resolution of the CASCADE detector is basically determined by the range of the decay products of ^{10}B , an α particle and a ^7Li nucleus, in the counting gas. As a practical estimate of the spatial resolution, the effective width of a stripe of the one dimensional readout structure was determined. This was done by scanning across a single channel using a narrow, collimated neutron beam.

The following measurement was carried out at the CT2 beam site at the ILL. The detector was placed on a table which was movable horizontally. This was used to successively irradiate different parts of the detector with a neutron beam that was

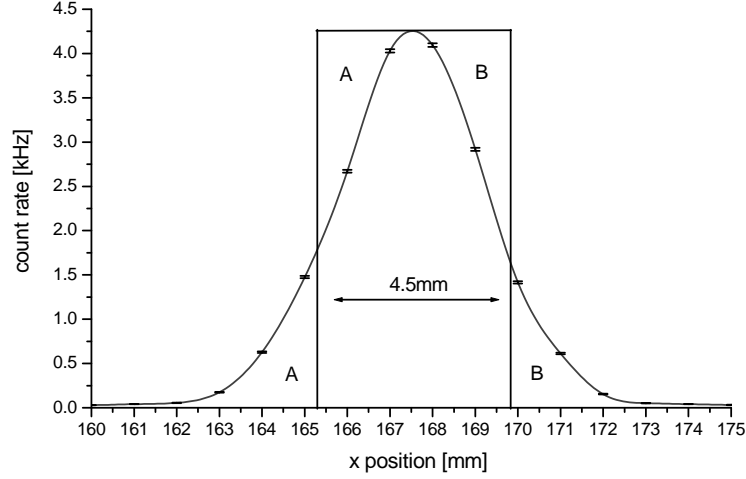


Figure 4.10: Scan of a single channel of an 1d readout structure with a neutron beam with a width of 0.5 mm.

limited in its profile by an aperture of a width of 0.5 mm.

The readouts stripes of a width of 3 mm were oriented vertically. The readout signal of a single readout stripe can be seen in figure 4.10. The profile of the scan was approximated by a spline. The effective width of the stripe was determined by matching the areas marked A and B. Numerical integration yielded a value of 4.5(1) mm. This value was used to integrate the spectrum obtained by the time-of-flight measurements at the PF1 beamline. This measurement is described in section 4.3.

4.2.3 Effective Dead Time Estimation

The finite amount of time required by the detector and the readout electronics to process a single detection event is called dead time of the detector. Two kinds of dead time have to be distinguished according to the way the arrival of further events influences the time of insensitivity of the detector. In case further events prolong the time of insensitivity the dead time is said to be *extendible*. Otherwise, it is called *non-extendible*.

The count rate r_m measured by a detector with purely non-extendible dead time τ is related to the true count rate r_0 by

$$\begin{aligned} \langle \text{number of true counts} \rangle &= \langle \text{number of measured counts} \rangle + \\ &\quad \langle \text{accumulated dead time} \rangle \times \langle \text{true count rate} \rangle \\ r_0 T &= r_m T + r_m T \tau r_0 = r_m T (1 + \tau r_0), \end{aligned}$$

where T denotes the counting period. Solving the equation above for r_m or r_0 yields:

$$r_m = \frac{r_0}{1 + r_0 \tau} \quad \Leftrightarrow \quad r_0 = \frac{r_m}{1 - r_m \tau}.$$

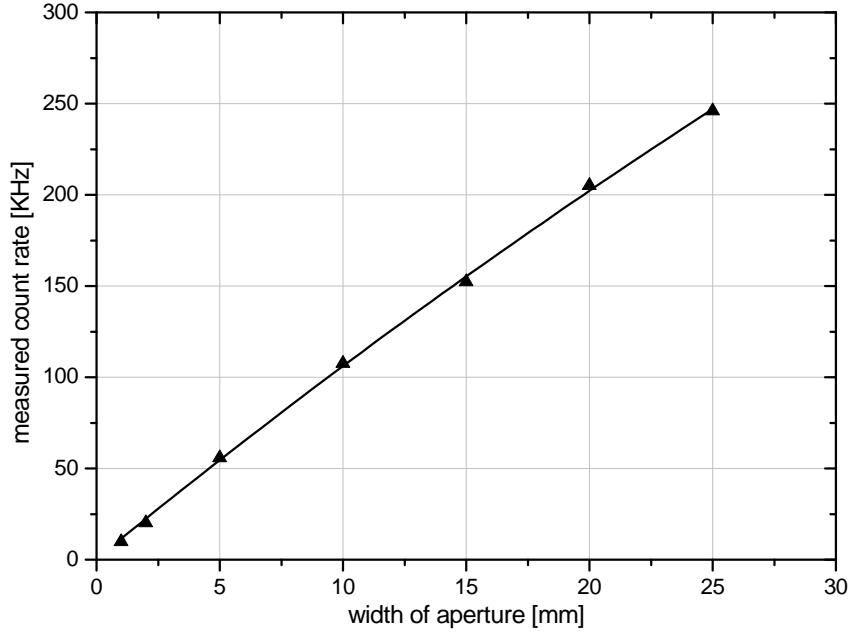


Figure 4.11: Experimental determination of the effective dead time of the ILL prototypes. A fit to the data yields $\tau = (450 \pm 120)$ ns. The statistical error bars are too small to be shown.

At low count rates of the CASCADE detector its dead time is likely to be dominated by the readout electronics. From [Bre99] it is known that GEM based detectors show saturation effects due to space-charge accumulation not prior to an event rate of 10^7 Hzcm⁻².

To measure the dead time of the CASCADE detector the following approach was taken: The detector was irradiated by a stable and monochromatic neutron beam. Apertures of different areas were successively inserted into the neutron beam. By that, the number of incident neutrons on the detector was varied. If the profile of the neutron beam is reasonably flat, a linear dependence of neutron intensity on the aperture area can be assumed. Using slit shaped apertures with a width x the true rate can be approximated as

$$r_0 = mx.$$

Any dead time measured this way obviously includes deviations from this assumption. The proportionality constant m is a measure for the neutron density in the beam. It is specific to the beam site.

Experimental Results

The effective dead time of one of the ILL CASCADE prototypes was determined at the CT2 neutron beam at the ILL in the way described above. Under the assumption

that the dead time is non-extendible the effective dead time τ of the system is given by

$$r_m = \frac{mx}{1 + mx/\tau} + r_b. \quad (4.1)$$

where r_b is the background count rate. The data measured are presented in figure 4.11. A least squares fit of equation 4.1 yields

$$\begin{aligned} m &= (11100 \pm 100) \text{ s}^{-1} \text{ mm}^{-1} \\ \tau &= (450 \pm 120) \text{ ns.} \end{aligned}$$

The background rate r_b was estimated from the count rate on the part of the detector that was not irradiated by the direct beam. Extrapolation to a vanishing aperture width yields:

$$r_b = (350 \pm 150_{\text{sys}}) \text{ s}^{-1}.$$

The result for τ is of the expected order. The large error is due to the small number of data points and the large uncertainty of the background rate r_b , which was apparently not measured sufficiently accurate. The dead time τ obtained here constitutes an upper limit. A decline in intensity of the beam at larger diameters would increase the dead time calculated since the incoming intensity would be overestimated.

The dead time of the CASCADE detector is dominated by the readout electronics as already mentioned before. Therefore any change of the electronics requires exact verification of its corresponding dead time. This measurement was done using a VV50 preamplifier, a D436 discriminator, a G43 gate generator and a DL630 counter [EW].

4.2.4 Rate Capability Tests

The PF1 site at the ILL offers a neutron flux ϕ of the order of $10^9 \text{ s}^{-1} \text{ cm}^{-2}$. To test the maximum rate capability of CASCADE detector, the ILL prototype (A) was irradiated by this continuous beam. An aperture of $20 \times 3.4 \text{ mm}^2$ limited the size of the neutron beam.

The readout electronics clearly was not able to cope with count rates higher than a few megahertz due to its large dead time, as shown in the preceding section. A current meter was used instead to monitor the incident currents on the readout structure directly. It was calibrated at low count rates by comparison with a digital rate meter.

At a count rate of 342 kHz a current of 10.5 nA was measured. The exposure of the detector to the full beam yielded a current of 3400 nA, which corresponds to a detection rate of about 110 MHz. The sensitive area of the detector was $5 \times 10 \text{ cm}^2$ and covered most of the beam profile.

The detector was subsequently irradiated by this intensity for about two hours without any influence on the functionality of the detector. There were no indications of detector aging. For the future, further long term irradiation test are planned.

4.3 Time of Flight Measurements at PF1

The PF1 beamline at the ILL is a site for fundamental physics experiments. It essentially is a bare beamline exit with no additional instrumentation. Currently the neutron density flux $d\phi/d\lambda$ at this beamline is under investigation for other experiments prospected. This was taken as a challenge to demonstrate the remarkable features of the CASCADE detector.

4.3.1 Time of Flight Measurements (TOF)

In this experiment the spectrum of the neutron beam was determined by a time of flight measurement. These measurements use the fact, that neutrons of different wave length travel with different velocities according to

$$v = \frac{h}{m_N \lambda},$$

where h denotes Planck's constant and m_N is the mass of the neutron. By chopping a continuous neutron beam into a pulsed beam, neutrons of different wave length can be distinguished by the time needed to traverse the flight path d from the chopper to the detector. The wave length information can be extracted from the arrival time t according to

$$t = \frac{d}{v} \Leftrightarrow \lambda = \frac{ht}{m_N d}, \quad (4.2)$$

under the assumption that all neutrons started at the same time, i.e. the pulse is infinitely short. With a finite pulse length, the spectrum convoluted with the pulse profile can be determined. The detector is connected to a TOF multichannel scaler, which sums up the events occurring in equal time intervals—the dwell time t_{dw} —within N_{sw} revolutions of the chopper.

4.3.2 Experimental Setup at PF1

The experimental setup for the time-of-flight measurements is shown in figure 4.12. The neutron beam enters the setup through the window of the neutron guide shown on the left. The continuous beam is converted into a pulsed beam by a chopper. A stack of paper is used as attenuator, which reduces the neutron flux by neutron absorption and incoherent scattering. After a flight path $d = 184$ cm, the neutrons are detected by a CASCADE detector. The stripes of the one dimensional readout structure have a width of 3 mm each. The detector is displaceable perpendicularly to the neutron beam and the readout stripe. This allows scans of the beam profile in x-direction, while integrating over the y-direction.

4.3.3 Neutron Flux

Each data point of the TOF spectra measured represents the number n of counts registered between time t and time $t + t_{dw}$ after the chopper opened. N_{sw} of such

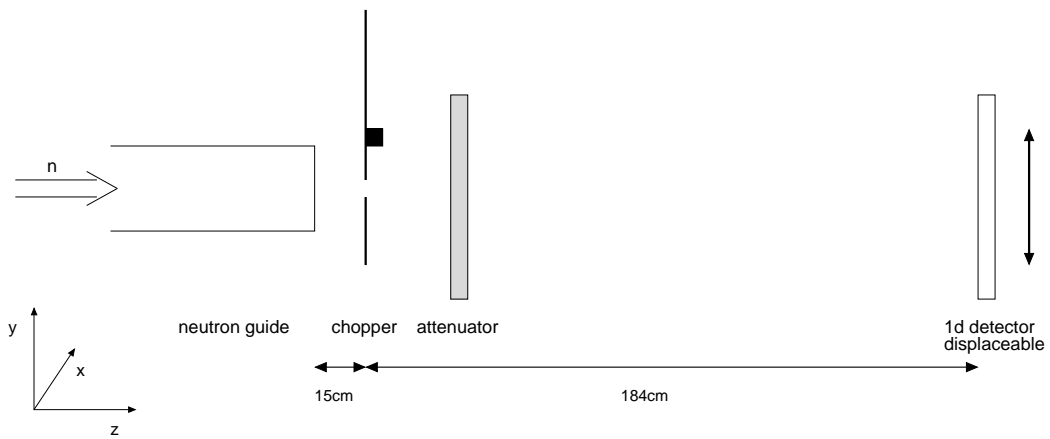


Figure 4.12: Experimental setup for the time-of-flight measurements at PF1, ILL

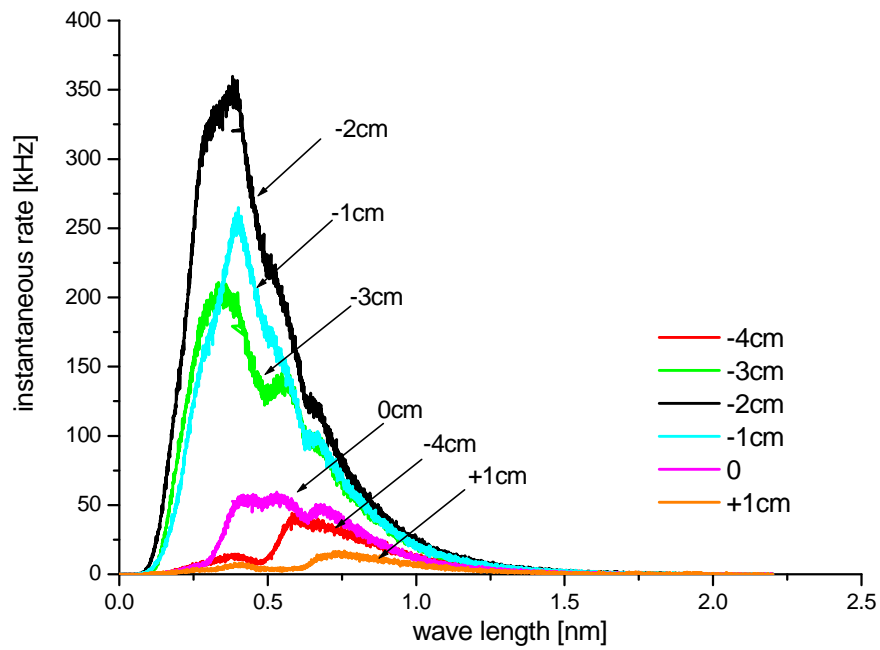


Figure 4.13: Instantaneous rate measured by the CASCADE detector on a single channel of the 1d readout structure at various horizontal displacements.

sweeps were accumulated. This yields an instantaneous rate r_i on the detector of

$$r_i = \frac{n}{N_{\text{sw}} t_{\text{dw}}}.$$

The instantaneous rates, as measured for several lateral positions x , can be seen in figure 4.13.

The instantaneous rate r_i , as a function of the flight time t_{flight} of the neutrons, is connected to the neutron flux $d\phi/d\lambda$ as follows:

$$r_i(t_{\text{flight}}) = \frac{d\phi}{d\lambda} \times \frac{d\lambda}{dt} \times \langle \text{constant factors} \rangle \times \langle \text{corrections dependent on } \lambda \rangle \\ \times \langle \text{corrections dependent on incident rate } r_0 \rangle. \quad (4.3)$$

The conversion factor from flight time t to wave length λ is given by

$$d\lambda = \frac{h}{m_N d} dt,$$

according to equation 4.2, where d is the distance between chopper and detector.

The instantaneous rate r_i denotes at any time t the rate detected by the detector during the revolution period t_{ch} of the chopper. The constant factors therefore include

- the open area of the chopper A_{ch} ,
- the revolution period of the chopper t_{ch} and
- the fraction of all incident neutrons transmitted by the chopper, the transmission coefficient T_{ch} .

The wave length dependent factors include

- the neutron detection efficiency $\mathcal{E}(\lambda)$ of the CASCADE detector,
- the transmission coefficient T_a of the attenuator used and
- the transmission coefficient $T_{\text{air}}(\lambda)$, which is due to the attenuation of the neutron beam by the air between the window of the neutron guide and the detector.

The only correction which depends upon the instantaneous count rate r_i is the dead time correction $C_d(r_i)$.

All of the above correction factors are discussed later in this section. The following equation includes these factors and is used to calculate the neutron density flux $d\phi/d\lambda$:

$$r_i(t) = \frac{d\phi}{d\lambda} \times \frac{d\lambda}{dt} \times t_{\text{ch}} T_{\text{ch}} A_{\text{ch}} \times \mathcal{E}(\lambda) T_a(\lambda) T_{\text{air}}(\lambda) \times \frac{1}{C_d(r_i)} \quad (4.4)$$

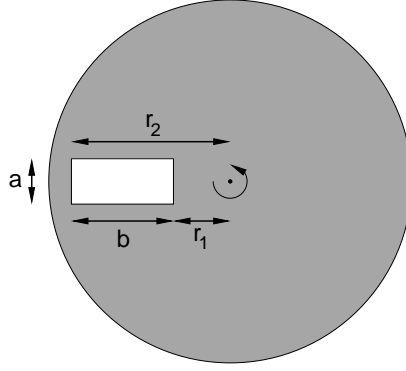


Figure 4.14: Geometry of the chopper used for the time-of-flight measurements. The height of the rotating slit is $a_1 = 3.4$ mm, that of the fixed slit $a_2 = 4.0$ mm. The width b of the slits is 20 mm. The radii are $r_1 = 54$ mm and $r_2 = 74$ mm.

The overall neutron flux ϕ can be obtained by integration over wave length λ :

$$\phi = \int \frac{d\phi}{d\lambda} d\lambda \quad (4.5)$$

The capture flux ϕ_c is a measure for the neutron density in the beam and emphasises contributions according to flight time through a given volume or, equivalently the wave length λ :

$$\phi_c = \int \frac{d\phi}{d\lambda} \frac{\lambda}{\lambda_0} d\lambda, \quad (4.6)$$

where $\lambda_0 = 1.8 \text{ \AA}$ is the wave length of thermal neutrons.

Chopper Transmission Coefficient T_{ch}

The chopper consists of two discs with slits, as can be seen in figure 4.14. The discs absorb any incident neutrons completely. One of the discs is fixed in place, while the other is rotating in front of it with a period of $t_{\text{ch}} = 23.12$ ms. The slits both have a width of $b = 20$ mm and their centre is located at a radius of $r = 64$ mm. They have slightly different widths of $a_1 = 3.4$ mm and $a_2 = 4.0$ mm, respectively.

The rotating chopper slit can be thought of being composed of rectangles of height dr and width a_1 . The time dependence of the fraction of neutrons transmitted through each of these rectangles $W(t, r)$ can be seen in figure 4.15. t_1 and t_2 are given by

$$t_1(r) = \frac{1}{2} \frac{a_2 - a_1}{2\pi r} t_{\text{ch}} \quad (4.7)$$

$$t_2(r) = t_1 + \frac{a_1}{2\pi r} t_{\text{ch}}. \quad (4.8)$$

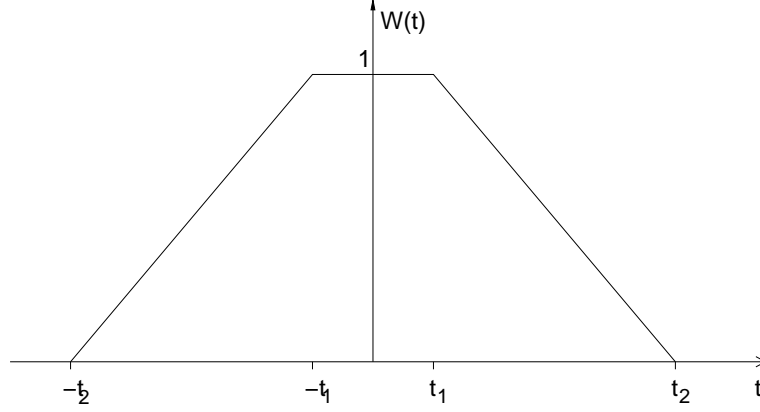


Figure 4.15: Fraction $W(t, r)$ of neutrons transmitted by a chopper slit of infinite height dr at radius r as a function of time. The trapezoidal shape is due to the different heights of the chopper slits. Identical slits would lead to a triangular shape.

$W(t)$ has a plateau due to $a_2 > a_1$. The depth l of the chopper slits, which is of the order of 1 mm, has been neglected as it has an influence only if $l \gg a$.

The fraction of neutrons transmitted by the chopper, the transmission coefficient T_{ch} , can be derived from $W(t, r)$:

$$\begin{aligned}
 T_{\text{ch}} &= \frac{1}{t_{\text{ch}}} \int_{r_1}^{r_2} \int_{-t_{\text{ch}}/2}^{t_{\text{ch}}/2} \frac{W(t, r)}{r_2 - r_1} dt dr = \int_{r_1}^{r_2} \frac{a_2}{2\pi b r} dr \\
 &= \frac{a_2}{2\pi b} \ln\left(\frac{r_2}{r_1}\right) \\
 T_{\text{ch}} &= \frac{1}{10\pi} (\ln 74 - \ln 54) \approx \frac{1}{100}.
 \end{aligned} \tag{4.9}$$

The maximum open area A of the chopper is determined by the smaller slit:

$$A_{\text{ch}} = a_1 \cdot b = 0.68 \text{ cm}^2. \tag{4.10}$$

Neutron Detection Efficiency $\mathcal{E}(\lambda)$

The ILL prototype A was used as detector for these measurements. Its neutron detection efficiency $\mathcal{E}(\lambda)$ was determined at CT2 beam site at the ILL. These measurements are discussed in section 4.2.1. Figure 4.9 shows the resulting wave length dependence.

Dead Time Correction $C_d(r_i)$

Inspection of the time of flight spectra showed saturation effects of the instantaneous rate at about 3 MHz. Any further increase in the incident neutron flux did not lead

to a change in rate. This is a clear sign for non-extendible dead time of the electronics (see section 4.2.3 for description). The dead time τ_d was therefore estimated from the maximum instantaneous rate obtained from measurements of the non-chopped beam:

$$r_{max} = (3.2 + 0.1) \text{ MHz} \quad \Rightarrow \quad \tau_d = \frac{1}{r_{max}} = (308 \pm 5) \text{ ns}$$

The dead time correction factor $C_d(r_i)$ for non-extendible dead time is given by:

$$C_d(r_i) = \frac{1}{1 - r_i \tau_d} \quad (4.11)$$

Air Transmission Coefficient $T_{\text{air}}(\lambda)$

Along the flight path between the window of the neutron guide and the detector, neutrons interact with the constituents of the air. Two main influences on the beam intensity can be identified:

- absorption of neutrons by nitrogen
- incoherent scattering by hydrogen in water vapor.

Both contributions lead to an exponential decay of the intensity of the neutron beam. The transmission coefficient T is given by

$$T(\lambda) = e^{-D\sigma_0 \frac{\lambda}{\lambda_0}},$$

where D denotes the area density of the absorber/scatterer and σ_0 is the cross section at $\lambda_0 = 1.8 \text{ \AA}$.

Approximately 80% of the constituents of air are nitrogen molecules N_2 . The area density D_N of nitrogen in air can be estimated from the ideal gas law as

$$D_N = 2 \cdot 0.80 \cdot \frac{px}{k_B T},$$

where p is the ambient gas pressure of $\approx 101.3 \text{ kPa}$, $x = 1.99 \text{ m}$ is the distance between the window of the neutron guide and the detector, k_B is Boltzmann's constant and $T \approx 300 \text{ K}$ the room temperature.

The hydrogen content of air is dominated by hydrogen contained in water molecules. The area density of these hydrogen particles D_H is given by

$$D_H = 2 \cdot h_r \frac{p_H x}{k_B T},$$

where $p_H \approx 3.2(9) \text{ kPa}$ is the vapour pressure of water at room temperature and h_r is the relative humidity of the air, which was about 80%.

The total transmission coefficient $T_{\text{air}}(\lambda)$ which includes both of these contributions, is given by

$$T_{\text{air}}(\lambda) = T_N(\lambda) \cdot T_H(\lambda) = \exp \left\{ - (D_N \sigma_{a,N} + D_H \sigma_{i,H}) \frac{\lambda}{\lambda_0} \right\}.$$

Insertion of the absorption cross section $\sigma_{a,N} = 1.90(3)$ barn of nitrogen and the incoherent scattering cross section $\sigma_{i,H} = 80.26(6)$ barn of hydrogen yields

$$\begin{aligned} T_{\text{air}}(\lambda) &= \exp \left\{ -(0.84 + 1.11) \cdot 10^{-2} \lambda [\text{\AA}] \right\} \\ &\approx \exp \left\{ -2.0 \cdot 10^{-2} \lambda [\text{\AA}] \right\}. \end{aligned} \quad (4.12)$$

Transmission Coefficient of the Attenuator T_a

During the time-of-flight measurements, two different attenuators had to be used to prevent the detector electronics from saturation. As is common practice for the attenuation of neutron beams, many sheets of paper were used. The attenuators 1 and 2 are two different sets of paper held together by staples.

The hydrogen content in these attenuators scatters the incident neutrons incoherently, i. e. the neutrons are scattered into 4π . This way the intensity in the direct neutron beam is reduced. The transmission coefficient T_a is wave length dependent and given by

$$T_a(\lambda) = e^{-\lambda/k}, \quad (4.13)$$

where k is the attenuation constant specific to the attenuator.

To determine the constants k_1 and k_2 of the two attenuators, time-of-flight measurements have been taken for all possible four combinations of attenuators (including no attenuator at all). These measurements were performed using a single readout channel of the one dimensional stripe. Low counting rates ensured that dead time effects of the detector did not disturb the measurements.

Insertion of two different attenuators into the beam should yield a transmission coefficient of the combination of

$$\begin{aligned} T_{a,1+2}(\lambda) &= T_{a,1}(\lambda) \cdot T_{a,2}(\lambda) \\ &= e^{-\lambda(1/k_1+1/k_2)}. \end{aligned}$$

The transmission coefficient of a single attenuator can then easily be extracted from the measurements using

$$T_{a,i}(\lambda) = \frac{T_{a,1+2}(\lambda)}{T_{a,i}(\lambda)} = \frac{I_{1+2}(\lambda)}{I_i(\lambda)},$$

where $I(\lambda)$ is the measured intensity at wave length λ . Figure 4.16 shows the results for both attenuators. From the data it is evident that equation 4.13 is not sufficient to describe the attenuators.

Instead

$$T_{a,j}(\lambda) = (1 - j_i)e^{-\lambda/k_i} + j_i, \quad i \neq j$$

which appears to describe the data much better, was fitted to the data. The data obviously contains some constant j_i and the factor $(1 - j_i)$ ensures that the stipulation $T_{a,i}(\lambda = 0 \text{ nm}) = 1$ is fulfilled. The fit yields:

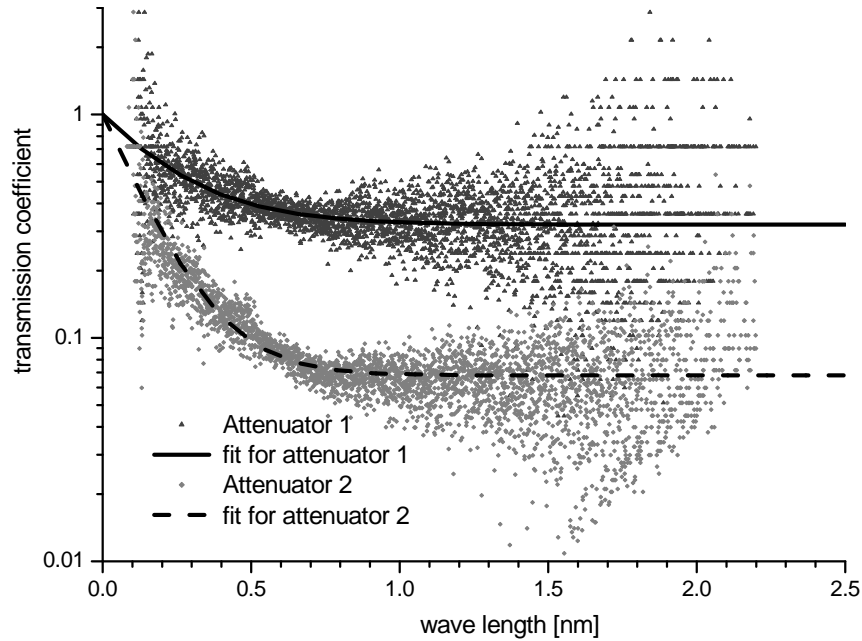


Figure 4.16: Transmission coefficient of the attenuators used at PF1.

	k_i	j_i
Attenuator 1	2.2692	0.321
Attenuator 2	1.4209	0.068

4.3.4 Experimental Results

In equation 4.13 it is assumed that all neutrons which are scattered by the attenuators are emitted into 4π . These neutrons should therefore no longer have a significant influence on the time-of-flight measurements. This is obviously not the case. Instead a fraction of the neutrons is moderated and the TOF spectrum is changed considerably. Hence, further analysis would not lead to reliable results.

Still these measurements revealed the potential of the CASCADE detector. Within a few sweeps of the chopper, the same statistic was achieved as would have been using a low pressure ^3He tube for hours. Additionally the complete beam profile was covered by the CASCADE detector. With a two dimensional readout structure equipped with the powerful CIPix chip the measurement could have been done even more quickly.

The high neutron detection efficiency of the ILL prototype (A) made the use of attenuators necessary. In future measurements attenuators based on gadolinium will be used. These will attenuate the neutron beam by absorption only.

The neutron flux $d\phi/d\lambda$ at $\lambda = 8.9 \text{ \AA}$ is of interest with respect to future neutron EDM experiments. A value can be derived from the data shown in figure 4.18 by

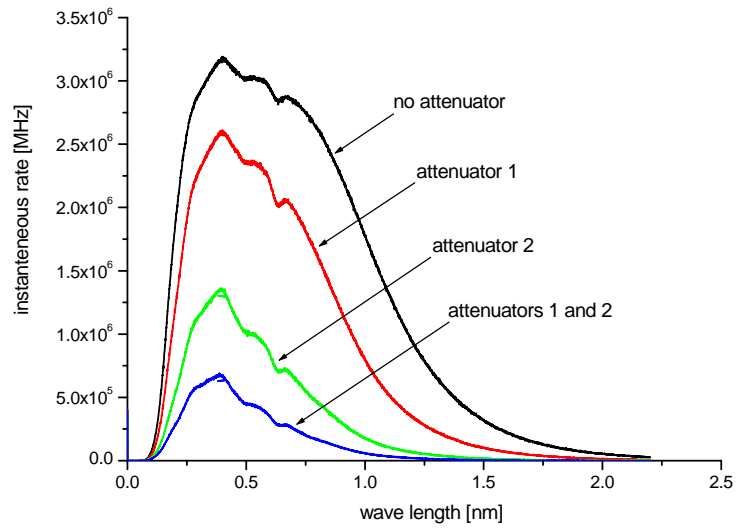


Figure 4.17: Instantaneous rates of the on the entire detector surface using different attenuators.

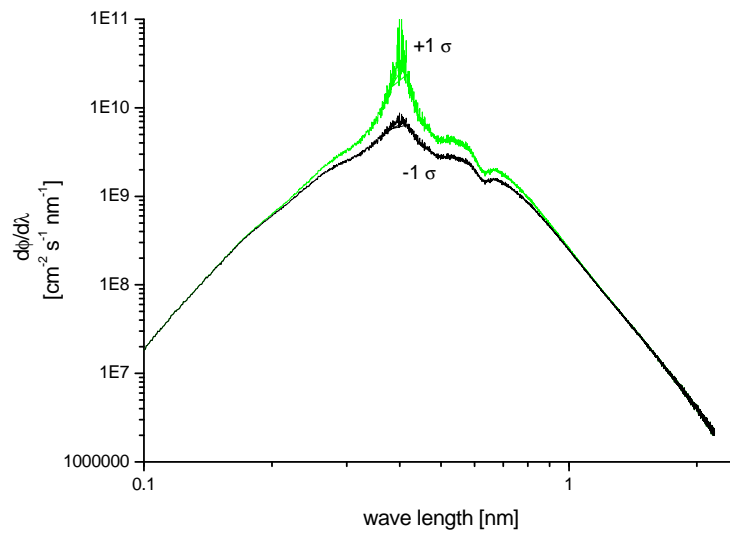


Figure 4.18: Neutron flux $d\phi/d\lambda$ as derived from the measurements without attenuator. The two curves correspond to the data margin of one σ in dead time correction.

extrapolation from very large wave lengths. This extrapolation will be insensitive to dead time corrections. The spectrum in this region is expected to fall as a power law. A fit to the data from 15 Å to 25 Å yields an exponent of -6.23 . Although elementary theory for a Maxwellian spectrum predicts an exponent of -5 the discrepancy could be attributed to the unknown influence of the two experimental setups upstream, which introduce a hole into the beamline. These experiments are also responsible for the structure encountered in the spectrum at 4.9 Å and 6.3 Å.

Finally this extrapolation yields a neutron flux $d\phi/d\lambda$ of

$$d\phi/d\lambda = (0.6 \pm 0.2) \cdot 10^9 \frac{1}{\text{cm}^2 \text{s nm}} \quad \text{at } 8.9 \text{ \AA}$$

The error on this result is dominated by the error in the air attenuation factor caused by the uncertainty in the vapour pressure.

5 Summary and Outlook

The CASCADE detector experienced a rapid evolution during the course of this diploma thesis. At the beginning it had become clear that the concept of the detector did indeed work. The transition to the modular design as described in chapter 2 was on its way. Just now it became possible to build, test and refine detectors in quick succession.

Several prototypes based on the modular design have been build as part of this thesis, each one improving upon the other. Consequently, the detector soon reached a stage such that serious tests with high neutron fluxes became necessary to prove its theoretical characteristics. Hence, they were tested with high neutron intensities at the Paul-Scherrer-Institut (PSI) as well as the Institute-Laue-Langevin (ILL). These tests showed that a small cascade of GEM-foils coated with ^{10}B can achieve a detection efficiency in the order of 15% for thermal neutrons. Consequently, up to 50% will be possible for an optimised and complete detector setup. Spatial resolution is found in the expected order of 4 mm.

The GEM technology has demonstrated its robustness and stable properties under the operating conditions of the CASCADE detector. Even when exposed to the highest neutron fluxes available in the world, no sparking or destruction of the detector occurred. Yet, a rate capability unknown to experimental neutron physics could be demonstrated.

To demonstrate the features of CASCADE detector, a small CASCADE beam monitor detector for the SANS instrument at the PSI was designed, constructed and tested as part of this work. It will yield valuable long term data on the CASCADE technology, which will help to further improve the CASCADE detector as a reliable instrument for neutron physics.

The improvements on the stability and efficiency of the detectors quickly revealed that the electronics had to be evolved as well. Hence, parallel to the construction and tests of prototypes, an detector readout concept from electronics to software was developed in the course of this thesis.

The new infrastructure allows full control of all relevant operating parameters, such as the gas flow and mixture, HV- and current-control on every single GEM-foil as well as the signal readout by an ASIC chip. All control- and readout electronics is integrated on a single VMEbus crate.

High energy physics pioneered processing of highest data rates. The CIPix chip developed originally for H1 is now employed for the CASCADE detector. It now allows to process highest count rates after being integrated into the supporting infrastructure.

The CASCADE detector has confirmed its high potential to become an general instrument in neutron scattering applications.

A Bus system glossary

A.1 VMEbus

The VMEbus in its original definition is an asynchronous, non-multiplexed bus which was defined in 1980 by Motorola, Mostek and Signetics corporations. The term *VME* stands for VERSAModule Eurocard, where VERSAModule is the original electrical description of the standard and Eurocard the mechanical form factor. The VMEbus offers the following basic features:

- master/slave architecture, including bus arbitration and multiprocessing
- address range of 16, 24 or 32 bits
- data path width of 8, 16 or 32 bits
- bandwidth up to 40 MBytes/s
- interrupt capability
- up to 21 slots on a single backplane

It has become industry standard, especially in the telecommunication business and is widely in use in high energy physics. Extensions for higher bandwidth, synchronous transfers and a data path width of 64 bits exist. [Pet00]

A.2 CAN bus

The Controller Area Network (CAN) is a serial communications protocol originally developed for passenger cars by Bosch [Bos91] and subsequently used in a wide variety of automotive and control applications. It offers the following basic features:

- physical bus length up to 40 m
- bandwidth up to 1 MBytes/s
- message based data transfer with an id length of 11 or 29 bits
- differential serial bus
- multi-master capability

- prioritised messages
- guaranteed latency times
- bus error detection and tolerance

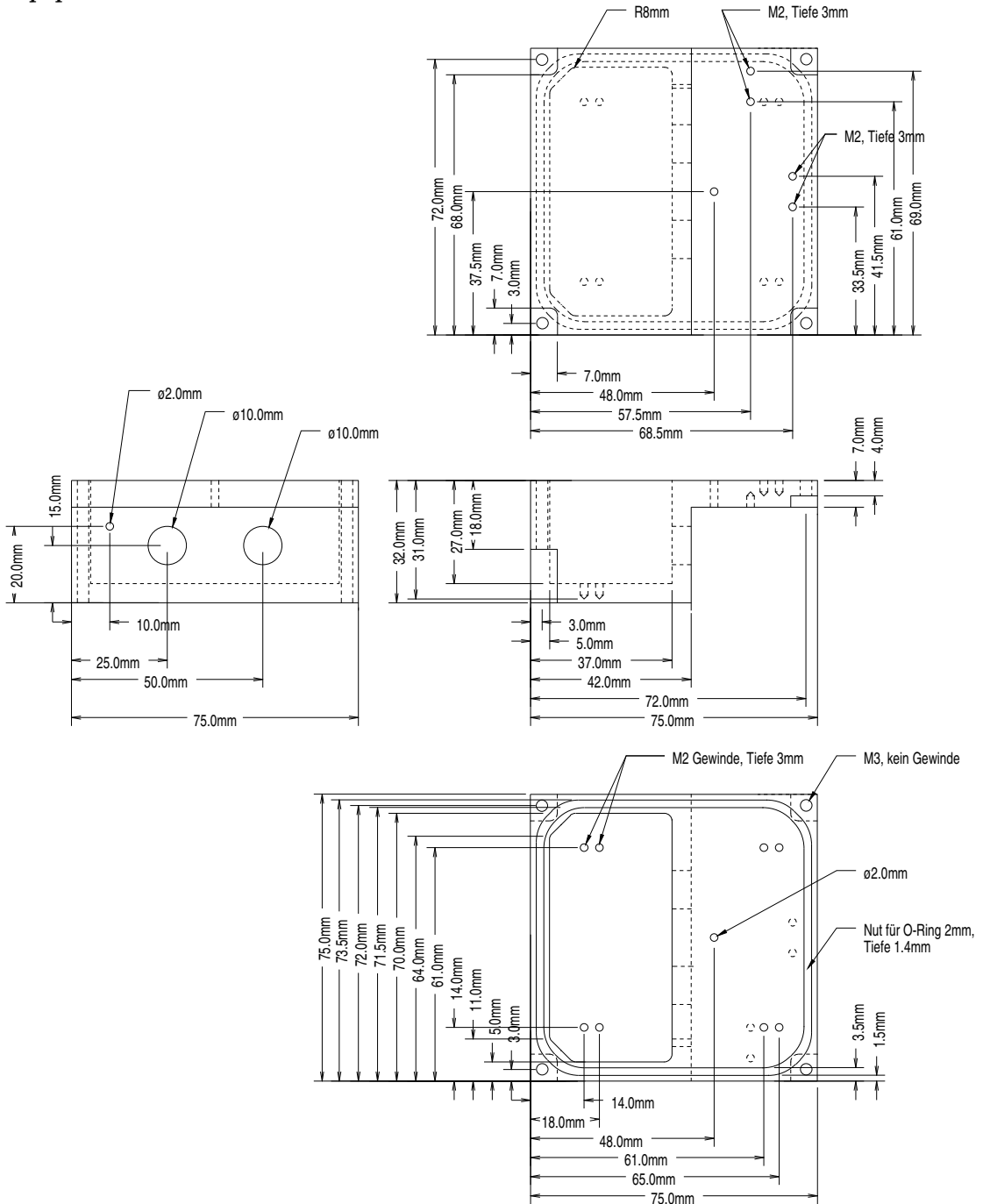
A.3 I²C-bus

The I²C-bus is a simple bi-directional 2-wire serial bus for efficient communication between integrated circuits (IC) defined by Philips in 1992 [Phi00], [Phi95]. Its basic properties are:

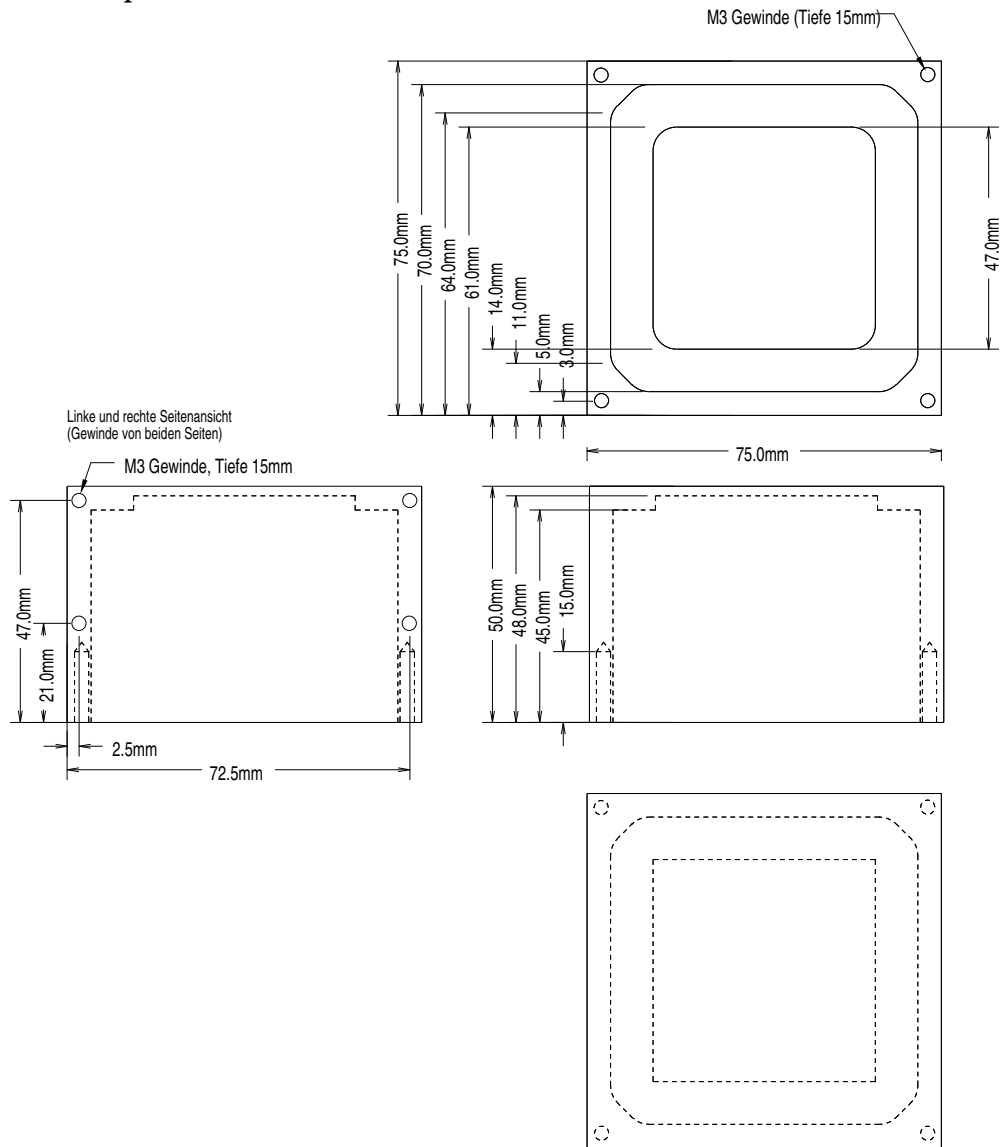
- two signal lines: a serial data line (SDA) and a serial clock line (SCL)
- every device on the bus is uniquely addressable by a 7 or 10 bit address.
- true multi-master bus including collision detection and bus arbitration
- transfer speeds of up to 100 kbit/s in standard mode. Advanced modes support transfer rates of up to 3.4 Mbit/s

B Drawings of the SANS beam monitor housing

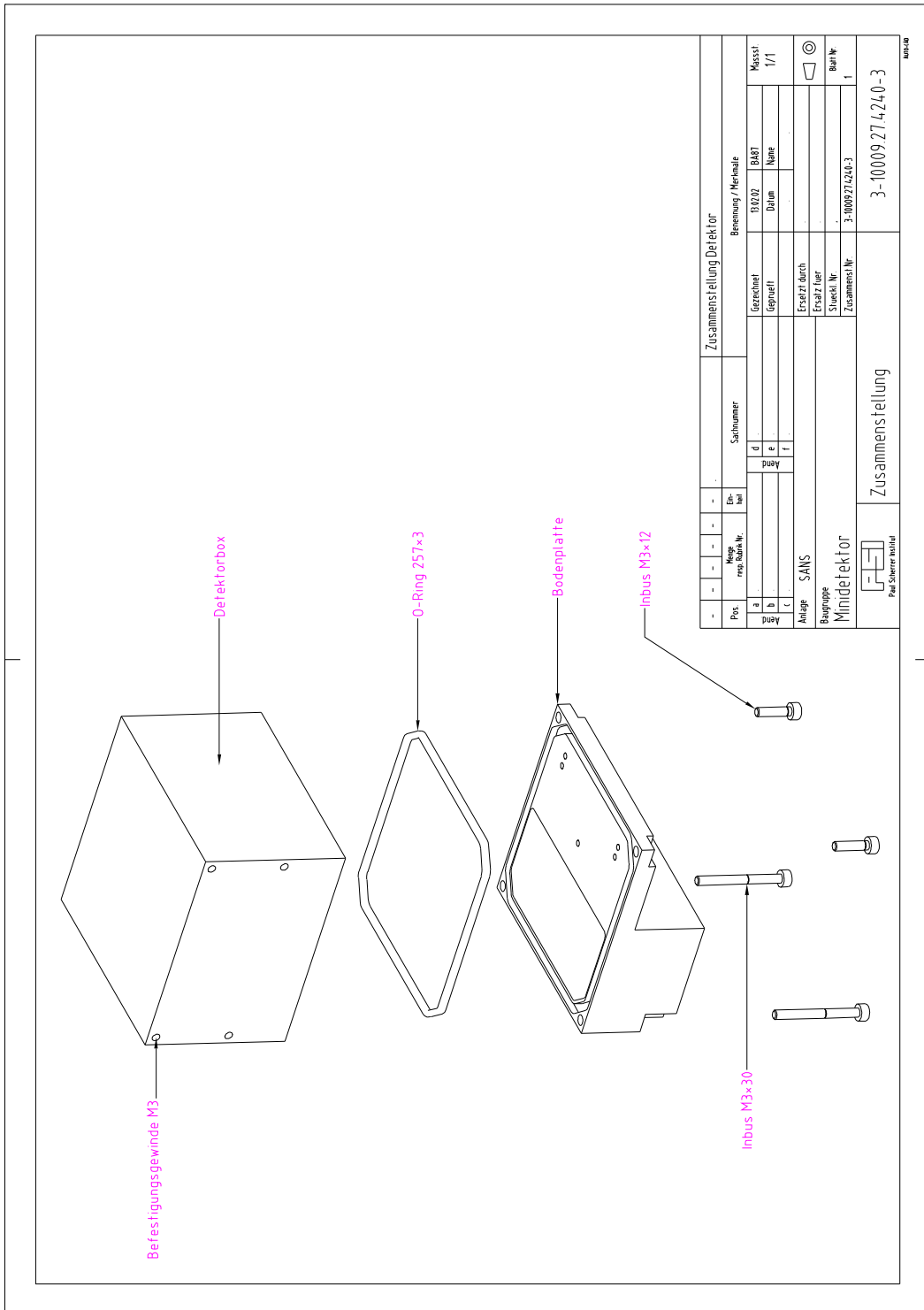
top part:



bottom part:



3D view:



Bibliography

- [Alt] ALTERA CORPORATION: (101 Innovation Drive San Jose, CA 95134)
- [ARW98] ARW-ELEKTRONIK, A. RAUSCH: *PCI-Bus to VMEbus Interface Type: PCI-VME*, version 1.1, 1998
- [ARW99a] ARW-ELEKTRONIK, A. RAUSCH: *Schnittstellenbeschreibung des Windows-NT Treibers PCIVME.SYS für das PCI-VME Interface von ARW-Elektronik*, 1999
- [ARW99b] ARW-ELEKTRONIK, A. RAUSCH: *Schnittstellenbeschreibung des Windows-95 Treibers VPCIVMED.VXD für das PCI-VME Interface von ARW-Elektronik*, 1999
- [Bau99] D. BAUMEISTER: *Entwicklung und Charakterisierung eines ASICs zur Kathodenauslese von MWPCs für das H1-Experiment bei HERA*, diploma thesis, University of Heidelberg, 1999
- [Bec64] K. H. BECKURTZ, K. WIRTZ: *Neutron physics*, Springer-Verlag, 1964
- [Ber98] J. BENLLOCH ET AL: *Further developments and beam test of the gas electron multiplier (GEM)*, Nucl. Instr. and Meth. A419 (1980) 410
- [Bit92] T. BITTER ET AL: *A long neutron optical horn for the ILL neutron-antineutron oscillation experiment*, Nucl. Instr. and Meth. A321 (1992) 284-290
- [Bos91] ROBERT BOSCH GMBH: *CAN Specification*, version 2.0, 1991
- [Bre99] A. BRESSAN, J. C. LABBÉ, P. PAGANO, L. ROPELEWSKI, F. SAULI: *Beam tests of the gas electron multiplier*, Nucl. Instr. and Meth. A425 (1999) 262
- [Bru02] H. BRUHNS: *Bau eines CASCADE-Neutronendetektors*, diploma thesis, University of Heidelberg, 2002
- [Cap01] M. CAPEANS: *Materials and gases: Lessons for detectors and gas systems*, review talk at the International Workshop on Ageing Phenomena in Gaseous Detectors, 2001
- [DuP02] DUPONT: *Kapton home page*, <http://www.dupont.com/kapton>

- [Cwe00] P. CWETANSKI: *Studies on detector prototypes for the inner tracking system of LHCb*, diploma thesis, University of Heidelberg, 2000
- [EW] ELEKTRONISCHE WERKSTATT DES PHYSIKALISCHEN INSTITUTS: Specifications and circuit diagrams, University of Heidelberg
- [Fio99] D. FIOJKA: *Entwicklung eines neuen Detektors für Neutronen*, diploma thesis, University of Heidelberg, 1999
- [Hil99] M. HILDEBRANDT: *Entwicklung und Bau der Detektoren für das Innere Spurkammersystem bei HERA-B*, dissertation, University of Heidelberg, 1999
- [HMI] B. GEBAUER: *Large-area micro-pattern detectors for thermal neutron imaging*, homepage, http://www.hmi.de/bereiche/SF/SF7/arbeitsg/thermal/index_en.html
- [Int95] INTEL CORPORATION: *8257 Serial Communications Controller – Controller Area Network Protocol*, 1995
- [Int96] INTEL CORPORATION: *8257 Serial Communications Controller – Architectural Overview*, 1996
- [Ise] ISEG SPEZIALELEKTRONIK GMBH: (D-01454 Rossendorf), <http://iseg-hv.de>
- [Ise01] ISEG SPEZIALELEKTRONIK GMBH.: *16 channel High Voltage Power Supply EHQ F 025x_503, Operators Manual*, version 2.06, 2001
- [Jan] JANZ AUTOMATIONSSYSTEME AG: (Im Doerener Feld 8, 33100 Paderborn), <http://www.janz.de>
- [Jan97a] JANZ COMPUTER AG: *VMOD-IO, VME MODULbus carrier board user's manual*, version 2.6, 1997
- [Jan97b] JANZ COMPUTER AG: *VMOD-FCAN, MODULbus CAN interface user's manual*, version 1.1, 1997
- [Kle00] M. KLEIN: *Experimente zur Quantenmechanik mit ultrakalten Neutronen und Entwicklung eines neuen Detektors zum orts aufgelösten Nachweis von thermischen Neutronen auf großen Flächen*, dissertation, University of Heidelberg, 2000
- [Kol01] M. KOLLEFRATH: *Atlas Drift Tube ageing tests*, talk at the International Workshop on Ageing Phenomena in Gaseous Detectors, 2001
- [Leo94] W. R. LEO: *Techniques for nuclear and particle physics experiments: a howto approach*, 2nd edition, Springer Verlag, 1994

- [Löc98] S. LÖCHNER: *Charakterisierung und Entwicklung eines CIP-Auslese-ASIC für das H1-Upgrade-Project 2000*, diploma thesis, University of Heidelberg, 1998
- [Neu92] Neutron News, Vol. 3, No. 3, 1992, pp. 29-37. (also available online at <http://www.ncnr.nist.gov/resources/n-lengths/>)
- [Pet00] W. D. PETERSON: *The VMEbus Handbook, A User's Guide to the IEEE 1014 and IEEE 821 Microcomputer Bus*, VMEbus International Trade Association, 1988
- [Pet00] W. D. PETERSON: *VMEbus Frequently Asked Questions*, <http://www.vita.com/vmefaq/index.html>, 2000
- [Phi95] PHILIPS SEMICONDUCTORS: *The I²C-bus and how to use it (including specifications)*, april 1995
- [Phi00] PHILIPS SEMICONDUCTORS: *The I²C-bus specification*, version 2.1, january 2000
- [Pri99] P. PRINZ AND U. KIRCH-PRINZ: *C++ Lernen und professionell anwenden*, MITP-Verlag, 1999
- [Ric99] C. RICHTER: *Development of Micro Pattern Gas Detectors for High Rate Experiments*, dissertation, University of Heidelberg, 2000
- [SAN02] PSI SANS homepage, <http://sans.web.psi.ch>, 2002
- [Sau97] F. SAULI: *A new concept for electron amplification in gas detectors*, Nucl. Instr. and Meth. A386 (1997) 531
- [Sau01] F. SAULI:, *Gas Electron Multiplier, Development and Applications*, talk at the RHIC Detector Workshop, <http://http://www.star.bnl.gov/STAR/rhicworkshop/agenda.html>, 2001
- [Sch02] K. SCHINDLER: *Entwicklung und Bau der Ausleseelektronik des CASCADE-Neutronendetektors*, Staatsexamensarbeit, University of Heidelberg, 2002
- [Sim01] F. SIMON: *Comissioning of the GEM Detectors in the COMPASS Experiment*, diploma thesis, Technische Universität München, 2001
- [Sta00] U. STANGE: *Charakterisierung und Weiterentwicklung des CIPix*, diploma thesis, University of Heidelberg, 2000
- [Urb00] M. URBAN: *Ein schneller Trigger für H1 bei HERA*, diploma thesis, University of Heidelberg, 2000

- [Wie] W-IE-NE-R, PLEIN & BAUS GMBH: (Müllersbaum 20, 51399 Burscheid), <http://www.wiener-d.com>
- [Zie99] M. ZIEGLER, P.CWETANSKI, U. STRAUMANN: *A Triple GEM detector for LHC-B*, LHC-B internal note TRAC 99-024, June 30, 1999